



1 **Temperature-enhanced effects of iron on Southern Ocean phytoplankton**

2

3 Charlotte Eich^{†,1,2,*}, Mathijs van Manen^{†,3}, J. Scott P. McCain^{4,5}, Loay J. Jabre^{4,6}, Willem H. v.d. Poll⁷, Jinyoung

4 Jung⁸, Sven B. E. H. Pont¹, Hung-An Tian³, Indah Ardiningsih³, Gert-Jan Reichart^{3,9}, Erin M. Bertrand⁴, Corina

5 P.D. Brussaard^{1,2,*}, Rob Middag^{3, 10}

6

7 [†]These authors contributed equally to this work.

8 Affiliations:

9 ¹Department of Marine Microbiology and Biogeochemistry, NIOZ Royal Netherlands Institute for Sea Research,

10 1797 SZ 't Horntje, The Netherlands

11 ²Institute for Biodiversity and Ecosystem Dynamics (IBED), University of Amsterdam, 1098 XH Amsterdam,

12 The Netherlands

13 ³Department of Ocean Systems, NIOZ Royal Netherlands Institute for Sea Research, 1797 SZ 't Horntje, The

14 Netherlands

15 ⁴Department of Biology, Dalhousie University, Halifax, Nova Scotia, Canada

16 ⁵Current Address: Department of Biology and Department of Earth, Atmospheric, and Planetary Sciences,

17 Massachusetts Institute of Technology, Cambridge, MA 02142, USA

18 ⁶Current Address: Marine Chemistry & Geochemistry Department, Woods Hole Oceanographic Institution,

19 Woods Hole, MA 02543, USA

20 ⁷CIO Oceans, Energy and Sustainability Research Institute Groningen, Faculty of Science and Engineering,

21 University of Groningen, Nijenborgh 7, Groningen, AG 9747, The Netherlands.

22 ⁸Korea Polar Research Institute, 26, Songdomirae-ro, Yeonsu-gu, Incheon 21990, Republic of Korea

23 ⁹Department of Earth Sciences, Faculty of Geosciences, Utrecht University, Utrecht, the Netherlands

24 ¹⁰Centre for Isotope Research-Oceans, Energy and Sustainability Research Institute Groningen, Faculty of Science

25 and Engineering, University of Groningen, 9712 CP Groningen, The Netherlands



26

27 *Correspondence to: Charlotte Eich (charlotte.eich@nioz.nl) & Corina Brussaard (corina.brussaard@nioz.nl)

28

29 **Short summary**

30 Phytoplankton growth in the Southern Ocean (SO) is often limited by low iron (Fe) concentrations. Sea surface
31 warming impacts Fe availability and can affect phytoplankton growth. We used Fe clean shipboard incubations
32 to test how changes in Fe and temperature affect SO phytoplankton. Their abundances usually increased with Fe
33 addition and temperature increase, with Fe being the major factor. These findings imply potential shifts in
34 ecosystem structure, impacting food webs and elemental cycling.

35

36 **Abstract**

37 Iron (Fe) is a key limiting nutrient for Southern Ocean phytoplankton. Input of Fe into the Southern Ocean is
38 projected to change due to global warming, yet the combined effects of a concurrent increase in temperature with
39 Fe addition on phytoplankton growth and community composition are understudied. To improve our
40 understanding of how Antarctic phytoplankton communities respond to Fe and enhanced temperature, we
41 performed four full factorial onboard bioassays under trace metal clean conditions with phytoplankton
42 communities from different regions of the Weddell and the Amundsen Seas in the Southern Ocean. Treatments
43 consisted of a combined 2 nM Fe addition with 2 °C warming treatment (TF), compared to the single factor
44 treatments of Fe addition at *in-situ* temperature (F), and non-Fe addition at + 2 °C (T) and at *in-situ* temperature
45 (C). Temperature had limited effect by itself but boosted the positive response of the phytoplankton to Fe addition.
46 Photosynthetic efficiency, phytoplankton abundances, and chlorophyll *a* concentrations typically increased
47 (significantly) with Fe addition (F and/or TF treatments) and the phytoplankton community generally shifted from
48 haptophytes to diatoms upon Fe addition. The < 20 µm phytoplankton fraction displayed population-specific
49 growth responses, resulting in a pronounced shift in community composition and size distribution (mainly towards
50 larger-sized phytoplankton) for the F and TF treatment. Such distinct enhanced impact of Fe supply with warming
51 on Antarctic phytoplankton size, growth and composition will likely affect trophic transfer efficiency and
52 ecosystem structure, with potential significance for the biological carbon pump.

53

<https://doi.org/10.5194/egusphere-2024-1508>

Preprint. Discussion started: 24 May 2024

© Author(s) 2024. CC BY 4.0 License.



54 Keywords: Antarctic algae, bioassays, size-fractionation, climate change, trace metals



55 **1. Introduction**

56 The Southern Ocean plays an important role in regulating the Earth's climate as it is an important sink for CO₂
57 (Takahashi et al., 2012; Friedlingstein et al., 2022; Fisher et al., 2023). Phytoplankton take up CO₂ and convert it
58 to biomass, forming not only the base of the pelagic food web but also driving the biological carbon pump
59 (Buesseler et al., 2020; Huang et al., 2023). During the short austral productive season, however, Antarctic
60 phytoplankton growth often becomes limited by low iron (Fe) availability (Martin et al., 1990; Boyd, 2002; Ryan-
61 Keogh et al., 2023). Fe is a vital micronutrient for a variety of cellular processes, including photosynthesis (Geider
62 & La Roche, 1994; Schoffman et al., 2016; Kroh & Pilon, 2020) and nitrate assimilation (Schoffman et al., 2016).
63 Shortage of Fe results in so called high nutrient, low chlorophyll (HNLC) conditions, where the ratio of
64 macronutrients, especially nitrate, relative to total Chlorophyll *a* (Chl *a*) concentrations is comparably high (Minas
65 & Minas, 1992; Sarmiento et al., 2004; Venables & Moore, 2010; Basterretxea et al., 2023). Trace metal supply
66 in the Southern Ocean follows a strong seasonal cycle where in winter Fe is replenished via deep water-mixing
67 (Tagliabue et al., 2014) or sediment resuspension in coastal areas (Boyd et al., 2012), but this supply is quickly
68 depleted again by phytoplankton uptake in the next season. However, Fe limitation for Antarctic phytoplankton
69 is predicted to be at least partially relieved in the future (Bazzani et al., 2023) because of enhanced Fe supply by
70 increased wind driven mixing (due to reduced ice-induced stratification) and sources associated with ice melt, i.e.,
71 glaciers (Annett et al., 2015; Sherrell et al., 2015; Van der Merwe et al., 2019; L. Seyitmuhammedov et al., 2022)
72 icebergs (Raiswell et al., 2008; Shaw et al., 2011; Raiswell et al., 2016; Hopwood et al., 2019) or sea-ice (Lannuzel
73 et al., 2016; Gerringa et al., 2020). These changes in Fe supply are associated with ongoing climate change that is
74 projected to lead to elevated temperatures and changes in wind patterns as well as associated currents and
75 upwelling (Turner et al., 2005; Moore et al., 2018). Overall, future Southern Ocean conditions will most likely be
76 warmer with potentially elevated Fe concentrations, which can be expected to also affect phytoplankton
77 productivity and community composition (Boyd et al., 2015; Laufkötter et al., 2015, Pinkerton et al., 2021).
78 Considering the urgency of warming and the anticipated change in Fe supply, there is a need for studies
79 investigating the combined effects of these two important drivers controlling phytoplankton growth in the
80 Southern Ocean. There are many reports on the effects of Fe addition to Fe-limited phytoplankton from the
81 Southern Ocean (Reviewed by e.g. Yoon et al., 2018; Bazzani et al., 2023) and several on the influence of
82 temperature (Reay et al., 2001; Morán et al., 2006; Boyd et al., 2013), but only few studies examined the combined
83 effects of Fe and temperature on Antarctic phytoplankton (i.e. Rose et al., 2009; Zhu et al., 2016; Andrew et al.,
84 2019; Jabre & Bertrand, 2020; Jabre et al., 2021; Aflenzer et al., 2023). In particular, studies using natural



85 phytoplankton communities are scarce (Rose et al., 2009; Jabre et al., 2021) and concentrated on Ross Sea
86 phytoplankton with relatively large temperature increases (3 to 6 °C). Hence, more insight into how phytoplankton
87 from other regional Antarctic seas respond to the warming projected by the year ~2100 (Meredith et al., 2019) is
88 needed.

89 The Weddell Sea is one of the key areas of dense Antarctic bottom water formation (Fahrbach et al., 2004) and
90 plays an important role in the global thermohaline circulation. The subpolar cyclonic Weddell Gyre circulating in
91 the Weddell Sea basin isolates the centre of the Weddell Sea from marginal Fe sources such as melt or sediments,
92 whilst the currents on the edges of the gyre have the potential to pick up Fe from a variety of sources, such as the
93 seafloor (Klunder et al., 2014; Sieber et al., 2021, Tian et al., in prep.). Generally, the Weddell Sea has a relatively
94 low primary productivity, associated with Fe limitation in the centre of gyre (Hoppema et al., 2007; Klunder et
95 al., 2014). In contrast, the west Amundsen Sea and specifically the Amundsen Sea Polynya (ASP) is known as
96 one of the most productive regions in the Southern Ocean in terms of net primary production per net area (Arrigo
97 & van Dijken, 2003). Additionally, this region (ASP) is characterised by a fast thinning of ice-sheets, shelf ice
98 and glaciers, with associated input of Fe required to sustain the high levels of primary productivity (e.g. Gerringa
99 et al., 2012; van Manen et al., 2022). Nevertheless, phytoplankton in the ASP could still be stimulated by
100 additional Fe input (Alderkamp et al., 2015).

101 The aim of the current study is to examine the concurrent effects of Fe supply and warming on Antarctic
102 phytoplankton communities from the Weddell Sea and the Amundsen Sea under controlled trace metal clean
103 conditions. Given the naturally low dissolved Fe (dFe) concentrations in the Southern Ocean, trace metal clean
104 conditions are crucial to avoid confounding Fe effects when studying temperature alone (Middag et al., 2023).
105 Our bioassay treatments comprised of Fe addition (F treatment), warming (T treatment), Fe addition and warming
106 (TF treatment) and the control (no Fe addition, no warming; C treatment). The temperature was enhanced by 2
107 °C, based on forecasts from the IPCC report (Meredith et al., 2019). Whilst the Amundsen Sea has shown a
108 warming trend over the past years already (Gómez-Valdivia et al., 2023; Drijfhout et al., 2024), the surface waters
109 of the Weddell Sea might not increase as much with climate change, but show short-term local temperature
110 increases (Darelius et al., 2023; Morrison et al., 2023; Teske et al., 2024). The concentration of dFe in the Fe
111 addition treatments (F and TF) was increased by 2 nM. Future Fe concentrations are highly uncertain (Hutchins
112 & Boyd, 2016; Tagliabue et al., 2016; Ryan-Keogh et al., 2023), and not necessarily linked to bioavailability of
113 Fe (Van Manen et al., 2022; Fourquez et al., 2023), but previous experiments in the Southern Ocean have shown
114 that such an addition represents (temporarily) Fe replete conditions (De Baar et al., 2005). Moreover, increased



115 Fe availability in the Southern Ocean could have a far-reaching impact, leading to increased nutrient consumption
116 consequently reducing nutrient transfer to lower latitudes where primary production is fuelled by these nutrients
117 (Primeau et al., 2013; Moore et al., 2018). By integrating biological and trace metal chemistry analyses within
118 large volume (20 L cubitainers), trace metal clean experiments, we aim to provide a clearer understanding of
119 future changes in phytoplankton growth patterns and the implications for the Southern Ocean's role in global
120 climate regulation.

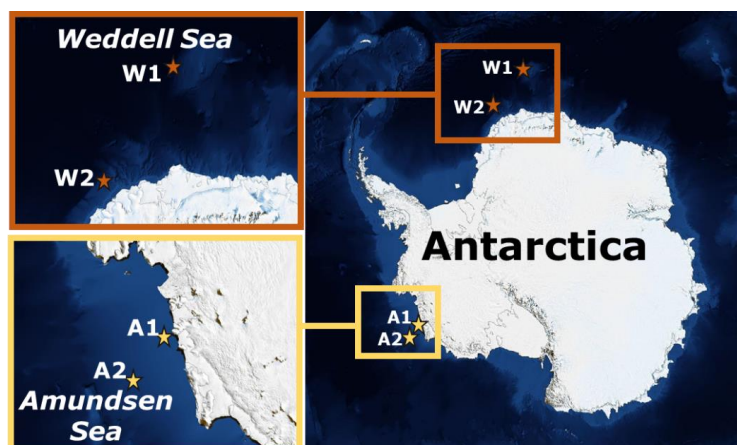
121

122 2. Material and Methods

123 2.1 Location and sampling

124 Natural seawater for the bioassays was collected during research expeditions (Fig. 1) in the Amundsen Sea
125 (bioassays A1 and A2, R/V Araon, ANA08B, 2017/18) and in the Weddell Sea (bioassays W1 and W2, R/V
126 Polarstern, Alfred-Wegener-Institut Helmholtz-Zentrum für Polar- und Meeresforschung (2017), PS117,
127 2018/19) in austral summer (December – February).

128



129

130 **Figure 1:** Location of the four bioassay experiments: Bioassays A1 and A2 were performed in the Amundsen Sea and W1 and
131 W2 in the Weddell Sea (Image obtained from NASA Worldview).

132

133 Seawater was sampled at the autofluorescence maximum (36 m for A2 and 20 m for both W1 and W2), except
134 for bioassay A1, which did not show an autofluorescence maximum and was sampled at the mid-mixed layer
135 depth (15 m). Water for each bioassay was collected in a single deployment of NIOZ's Titan ultraclean CTD
136 sampling system for trace metals (De Baar et al., 2008), mounted with pristine large volume samplers (Rijkenberg



137 et al., 2015). To prevent light shock for the phytoplankton, the original PVDF Pristine samplers were replaced by
 138 a light-proof poly-propylene version. Salinity (conductivity), temperature, fluorescence, depth (pressure) and
 139 oxygen were measured with a CTD (Seabird SBE 911+) mounted on the trace metal clean sampling system (De
 140 Baar et al., 2008). To avoid contamination, further processing was performed under trace metal clean, dimmed
 141 light conditions and at 2 °C in a cleanroom environment inside a modified high-cube shipping container which
 142 fits the Titan sampling system.

143 Water for Amundsen Sea bioassay A1 was sampled from the middle of the Amundsen Sea Polynya (ASP) and for
 144 bioassays A2 in the marginal sea ice zone just outside of the ASP. Both W1 and W2 were performed with water
 145 from the eastern Weddell Sea. The Amundsen Sea bioassays A1 and A2 ran for 6 days (25 to 31 January and 31
 146 January to 6 February 2018, respectively), whilst the Weddell Sea bioassays W1 and W2 ran for 8 days (28
 147 December to 5 January and 9 to 17 January 2019, respectively). See Table 1 for *in-situ* environmental conditions
 148 at sampling depth (at the start of the bioassays). The *in-situ* temperature was below zero for all bioassays, with
 149 lowest values for A2 and W2 (-1.6 °C and -1.4 °C, respectively, compared to -0.6 °C and -0.3 °C for A1 and W1).
 150 The daily average irradiance at sampling depth on day of sampling was lowest for A1 and A2, i.e., < 6 μmol
 151 quanta m⁻² s⁻¹, compared to 18 and 98 μmol quanta m⁻² s⁻¹ for W1 and W2.

152 **Table 1:** Characteristics of the seawater used for the bioassay experiments. Lat. = latitude, Long. = longitude, Temp =
 153 temperature, Si = silicate, PO₄ = phosphate, NO_x = nitrate + nitrite, Fe = iron, Chl a = chlorophyll a, Phyto = total flow
 154 cytometry based phytoplankton abundances, F_v/F_m = photosynthetic capacity of the total phytoplankton. The reported
 155 irradiance is the average irradiance at the sampling depth on the day of sampling.

Bioassay	Station	Lat. (°S)	Long. (°W)	Temp. (°C)	Salinity (psu)	Irradiance (μmol quanta m ² sec ⁻¹)	Si (μM)
A1	31	73.50	116.50	-0.6	33.99	5.0	84.7
A2	52	72.00	118.42	-1.6	33.89	3.1	78.5
W1	17	65.00	000.00	-0.3	33.90	17.7	58.3
W2	36	70.08	011.08	-1.4	33.82	97.6	27.7

Bioassay	PO ₄ (μM)	NO _x (μM)	Fe (nM)	total Chl a (μg L ⁻¹)	< 20 μm Chl a (%)	Phyto (x10 ³ mL ⁻¹)	F _v /F _m r.u.
A1	1.8	27.7	0.28	3.0	42	8.4	0.6
A2	2.1	30.9	0.10	0.4	98	7.1	0.6
W1	1.6	24.0	0.05	1.5	24	5.6	0.3
W2	1.9	27.9	0.03	0.6	65	4.4	0.3



157 **2.2 Bioassay incubation set-up**

158 Collapsible 20 L cubitainers (LDPE with PP caps and fitted with PE faucet; Cole-Palmer, Illinois, USA) were
159 used for the bioassay incubations. These were soap and HCL (1 M) cleaned prior to the expeditions and stored
160 with full surface contact in 0.024 M HCl (VWR Normatom Ultrapur, Avantor, Radnor, USA) for at least two
161 months. Before use, cubitainers were rinsed five times with ambient seawater. The natural seawater for the actual
162 incubations was distributed randomly to the total of 12 cubitainers which were then randomly assigned to the
163 different treatments. Trace metal clean conditions were maintained during all sampling and sample handling.

164 The bioassay treatments (performed in triplicate) were: *in-situ* conditions (control, C), + 2 nM dFe (as FeCl₃)
165 addition (F), + 2 °C temperature increase (T), and + 2 nM dFe addition and + 2 °C temperature increase (TF). For
166 the Amundsen Sea bioassays, a natural isotopic composition (natural dFe) was used for the dFe addition, whilst
167 d⁵⁷Fe was used in the Weddell Sea bioassays. This practice was adopted to better differentiate the added Fe from
168 the naturally present Fe, as we noticed that the dFe concentration in Fe amended Amundsen Sea bioassays quickly
169 returned to background concentrations (see section 3.1). Measuring Fe with a natural isotopic composition at these
170 low concentrations is still a challenge and combined with inherent variability between replicates. After several
171 days it became impossible to distinguish the Fe amended and non-amended treatments in Amundsen Sea bioassays
172 based on their natural dFe concentration (see section 3.1). The variation in natural dFe expected between Fe
173 amended and non-amended treatments despite precipitation and uptake, was hidden in the analytical and
174 environmental variability. For Weddell Sea bioassays we thus decided to add ⁵⁷Fe, a rare (2.12 % abundant vs
175 91.75 % for ⁵⁶Fe) natural isotope of Fe. Given its low natural abundance, ⁵⁷Fe is not nearly as sensitive to analytical
176 and replicate variation as such variation is insignificant relative to the addition, allowing better insight in Fe
177 drawdown over the course of the experiments.

178 Average starting concentrations of dFe in the Fe addition treatments ranged from 2.03 to 2.28 nM for both Weddell
179 and Amundsen Sea bioassays. Temperatures in the T and TF treatments were 1.4, 0.4, 1.7 °C and 1 °C, for A1,
180 A2, W1 and W2, respectively (see Table 1 for an overview of starting conditions in all treatments). One replicate
181 of the control treatment in bioassay W1 started leaking during the incubation and was thus not sampled from day
182 4 onwards. For bioassay W2, the *in-situ* temperature of -1.4 °C could not be maintained due to the very sunny
183 weather, resulting in an increase of 0.4°C for all treatments., Final incubation temperatures were -1.0 °C in the
184 control (C) and Fe-only (F) treatment and 1 °C (instead of 0.6 °C) in the T and TF treatments. This temperature
185 adjustment was done slowly over the course of 24 h on the second day of the incubation. More details about the



186 set-up can be found in the supplemental data (Fig. S1, supplement Bioassay Setup). Over the course of the
187 incubation period, temperatures were kept constant, with a maximum temperature fluctuation of ± 0.3 °C.
188 For Amundsen Sea bioassays, light levels were chosen to mimic *in-situ* conditions, but noting the low light
189 conditions during these incubations (ca. 3 % of in-air photoactive radiation, PAR; i.e. average 3.4 and 1.5 μmol
190 quanta $\text{m}^{-2} \text{s}^{-1}$ for A1 and A2 over the course of incubation), we opted for non-limiting light conditions (Bertrand
191 et al., 2011) for the (later performed) bioassays of the Weddell Sea (ca. 12 % of in-air PAR; i.e. average 69 and
192 100 μmol quanta $\text{m}^{-2} \text{s}^{-1}$ for W1 and W2 over the course of incubation). The percentages and values reported refer
193 to approximate light conditions within cubitainers. Samples for dissolved and particulate metals, Chl *a*, pigment-
194 based taxonomic analyses, and particulate organic carbon (POC), nitrogen (PON) and phosphate (POP) were
195 taken before filling of the cubitainers at the start of the bioassay incubations (t_0), and at the end of the incubations
196 after 6 (Amundsen Sea) or 8 (Weddell Sea) days. Samples for phytoplankton photosynthetic efficiency (F_v/F_m)
197 and phytoplankton abundances were taken at least every other day. Macronutrients were measured on board at
198 least every other day to screen for potential macronutrient limitation.

199

200 **2.3 Setup verification**

201 To test for potential Fe contamination, three cubitainers were filled with ultrapure (UP) water and handled and
202 subsampled using the same methods and frequency as the treatments. Subsamples for dFe analysis were taken at
203 the start (0.08 ± 0.04 nM) and after three (0.07 ± 0.04 nM) and six (0.06 ± 0.04 nM) days. Concentrations of dFe
204 stayed consistently low, suggesting minimal or no contamination. We also tested whether added dFe stayed in
205 solution or adsorbed to the cubitainer walls and found a slow gradual decrease over the first few days in dFe
206 concentrations after addition to UP water that we attribute to precipitation and wall adsorption (Table S1). During
207 our experiments, the concentrations of added dFe decreased more rapidly, whereas the dFe concentrations in the
208 non-Fe treatments, as well as the non-added form of dFe in Fe treatments ($d^{57}\text{Fe}$ for Amundsen and natural dFe
209 for Weddell Sea bioassays), stayed low and relatively constant over time. Since phytoplankton grew in all
210 treatments, the faster decrease of added dFe was likely due to uptake and sorption onto (biogenic) particles rather
211 than precipitation to the cubitainer walls. Low traceable amounts of $d^{57}\text{Fe}$ during the second half of the incubations
212 in W1 and W2 suggested that the initial decrease in Fe concentrations did not correspond to permanent removal
213 from the bioavailable Fe pool (e.g. due to absorption; Jensen et al., 2020) but instead buffered the dissolved pool
214 (as suggested for natural settings with exchange between the (labile) pFe and dFe pools; Van Manen et al., 2022),



215 or that most of the added Fe was taken up by phytoplankton as rapid luxury uptake during the first days of an
216 experiment (Lampe et al., 2018).

217

218 **2.4 Macronutrients**

219 During the Amundsen Sea bioassays, dissolved macronutrients were measured onboard following Jeon et al.
220 (2021), according to the Joint Global Ocean Flux Study (JGOFS) protocols (Gordon et al., 1993) using a four-
221 channel Auto-Analyzer (QuAAtro, Seal Analytical, Norderstedt, Germany). Measurement precisions were ± 0.02 ,
222 ± 0.28 and ± 0.14 μM for phosphate, silicic acid, and nitrogen (nitrate + nitrite), respectively (Jeon et al., 2021).
223 For Weddell Sea bioassays, samples for nitrate, nitrite, phosphate, and silicic acid were measured following the
224 method described by Gerringa et al. (2019). Measurements precisions were ± 0.01 , ± 0.31 and ± 0.04 μM for
225 phosphate, silicic acid, and nitrogen (nitrate + nitrite), respectively.

226

227 **2.5 Dissolved and particulate metals**

228 Cubitainers were subsampled for dFe as well as other dissolved trace metals (dMn, dCo, dCu, dNi, dZn, dCd)
229 using a 0.2 μm Sartobron-300 filter cartridge (Sartorius AG, Göttingen, DE) for bioassay A1 and A2 and pre-acid
230 cleaned 0.2 μm Acropak filter cartridges (Cytiva, Marlborough, USA) for W1 and W2. Filters were fitted to an
231 UP-cleaned vented PE faucet attached to the cubitainer with HCl acid (1.5 M) cleaned silicon tubing. Filtered
232 samples were taken by applying pressure to the cubitainer. Different filters were used for Fe replete and deplete
233 treatments, and filters were replaced between experiments. The dissolved trace metal samples were collected in
234 acid cleaned 125 mL LDPE bottles following GEOTRACES protocols (Cutter et al., 2017) and directly acidified
235 by adding ultra-pure HCl (Baseline®HCl; Seastar Chemicals Inc, Sidney, CA), resulting in a concentration of
236 0.024 M with a final pH of ~ 1.8 . Samples were stored until analysis at NIOZ. Trace metal samples were prepared
237 and analysed following van Manen et al. (2022) and references within. In short, trace metal samples were
238 pre-concentrated using a SeaFAST pre-concentration system (ESI). Blank contributions from sample handling,
239 pre-concentration, and analysis steps were determined by analysing acidified MQ water (~ 1.8 pH) prepared in the
240 same way as real samples.

241 For particulate trace metals (pMn, pCo, pCu, pNi, pZn, pCd) and POP, 25 mm poly-ether-sulfone (PES) disc
242 filters (0.45 μm Pall Supor, Port Washington, USA) and polypropylene filter holders (Advantec, Cole-Parmer,
243 Vernon Hills, USA) were used, following the protocol adapted by Van Manen et al. (2022) with one additional
244 step: samples were soaked for at least 30 minutes in oxalate-EDTA (respectively 0.75M and 5.5M) in a 10L carboy



245 (VWR Collection; Avantor, Radnor, USA) to remove all trace metals outside or adsorbed to phytoplankton cell
246 walls (modified after Hassler & Schoemann, 2009) and subsequently filtered. Due to time limitations, samples for
247 particulate metals were only taken during experiment A1, W1 and W2. Filters were stored frozen at -20 °C until
248 analysis. In the NIOZ lab, filters were treated with two successive digestion steps to determine the total particulate
249 fraction. All vials used in the digestion procedures were rigorously cleaned with HF and HCl beforehand and
250 rinsed with UP water. Filters were subjected to a leach consisting of 1.8 mL of 4.35M (25 %) two times sub-boiled
251 distilled acetic acid and 0.02M (2 %) hydroxylamine hydrochloride (99.999 % trace metal basis, Sigma-Aldrich,
252 Saint-Louis, USA). Subsequently, filters were digested following the total digestion protocol developed by Cullen
253 & Sherrell (1999) and modified by Planquette & Sherrell (2012). A volume of 2 mL of 3 × sub-boiled distilled
254 8.0 M (50 %) HNO₃ (VWR Chemicals – AnalaR NORMAPUR, Avantor, Radnor, USA) and 2.9 M (10 %) HF
255 (Merck – Supelco, Kenilworth, USA) was added. The vials were closed tightly and refluxed for 4 h at 110 °C.
256 The solution was then transferred to a secondary Teflon vial and were then heated to near dryness at 110 °C. A 1
257 mL volume of 8.0 M (50 %) 3× sub-boiled distilled HNO₃ (VWR Chemicals– AnalaR NORMAPUR, Avantor,
258 Radnor, USA) and 15 % H₂O₂ (Merck – Suprapur, Kenilworth, USA) was added to the dried vial contents. The
259 vials were refluxed for 1 h at 110 °C and subsequently cooled to room temperature. Addition of reagents and
260 refluxing were repeated once. After this repetition, the vials were heated to near dryness at 110 °C. The samples
261 were re-dissolved in 2 mL 1.5 % 3× sub-boiled distilled HNO₃ with 10 ppb Rh as internal standard and transferred
262 to 2 mL Cryovials® (VWR, Avantor, Radnor, USA) for storage and analysis.

263

264 **2.6 ICP-MS trace metal measurements and particulate organic phosphorous**

265 Dissolved trace metal samples were pre-concentrated using a SeaFAST pre-concentration system (ESI) using two
266 loops of 10 mL and were eluted into 350 µL elution acid (1.5 M Teflon distilled HNO₃ with rhodium as internal
267 standard) which gives a pre-concentration factor of 57.14 (see van Manen et al., 2022). Dissolved trace metal
268 samples, blanks (Supplementary Table S2), and references (Table S3) were analysed by ICP-MS (Thermo
269 Scientific Sector Field High-Resolution Element 2, Thermo Fisher-Scientific, Waltham, USA). Blank values were
270 much lower than the analysed samples, and reference results were in good agreement with certified values.
271 For the particulate samples, including POP, the procedure blanks without a filter were treated identically to the
272 samples, except for the steps involving filter handling and the removing of the filter from the filter holders.
273 Therefore, the vial blank is included in this reagent blank. Filter blanks consisted of unused acid cleaned PES disc
274 filters (Table S4).



275 Accuracy and precision of the digestions were assessed by Certified Reference Materials (CRMs). There is no
276 CRM available for marine suspended particulate matter, therefore accuracy could only be approximated by
277 analysis of other available CRMs. PACS-2 and MESS-3 (marine sediments, National Research Council of
278 Canada) were analysed. For each CRM, 10-30 mg were digested, whilst recommended sample weights are 250
279 mg for PACS-2 and MESS-3. The lower sample weights in this study were chosen to be representative of actual
280 marine particulate suspended matter concentrations (similar to Ohnemus et al., 2014). PACS-2 and MESS-3 were
281 only subjected to the total digestion (Table S5). The CRMs were in good agreement with the certified values.

282

283 **2.7 Particulate organic carbon and nitrogen**

284 For POC and PON sampling, 1 L of unfiltered seawater was collected from each cubitainer and stored in dark
285 bottles (Nalgene, Rochester, USA) at 1 °C until further processing (within 4 h after sampling). Filtrations were
286 then performed using combusted (4 h at 500 °C; Verardo et al., 1990) 0.3 µm 25 mm GF75 filters (Whatman,
287 Cytiva, Maidstone UK) and under modest under pressure (max. 200 mbar). Filters were folded once, packed in
288 aluminium foil, and stored frozen (-20 °C) until analysis. The POC and PON concentrations were measured using
289 a Thermo-Interscience Flash EA1112 Series Elemental Analyzer (Thermo Scientific, Waltham, USA) with excess
290 oxygen, at 900 °C and a detection limit of 100 ppm and a precision of 0.3 % (Verardo et al., 1990). Before analysis,
291 GF75 filters were folded and packed into a tin cup. The instrument blank is included by the analyser calibration.
292 Carbon and nitrogen content of samples and blanks were computed according to the results of the standard
293 measurements, and the blank was subtracted from the sample. Acetanilide (C₈H₉NO) with 71.09 % C and 10.36
294 % N (ThermoQuest, Milan, Italy) was measured as standard material, and silty and sandy soil standards from
295 Elemental Microanalysis were measured as an internal reference.

296

297 **2.8 Phytoplankton photosynthetic efficiency**

298 F_v/F_m was determined in a Water-K quartz cuvette (3.5 mL) using pulse amplitude modulated fluorometry (Heinz
299 Walz WATER-PAM, with Red LEDWATER-ED cuvette version S/N EDEE0196, Walz GmbH, Effeltrich,
300 Germany). Samples were kept in 50 mL Greiner tubes (Thermo Fisher-Scientific, Waltham, USA) in the cold
301 (stored in a cool box on ice) and in the dark for dark-adaptation (15 min up to occasionally 4 h). Acclimation
302 times of up to 4 h did not affect photosynthetic efficiency of different phytoplankton (L. Peperzak, personal
303 communication; Eich et al., 2021). The cuvette was rinsed with ultra-pure (UP) water between samples and the
304 relative fluorescence yield (F_t) values were kept between 100 and 1000 by adjusting the PM-gain. Blanking was



305 done for each station and/or bioassay using 0.2 μm filtered seawater from the respective stations and repeated
306 after PM-gain adjustment when needed. The following formula was used to obtain the photosynthetic efficiency:
307 $F_v/F_m = (F_m - F_0)/F_m$, with F_0 being the minimum fluorescence, and F_m being the maximum fluorescence.

308

309 **2.9 Chlorophyll a concentration and pigment-based taxonomic analyses**

310 Samples (0.54 - 2.65 L) for Chl *a* concentrations and pigment-based community composition were filtered within
311 30 min of subsampling (kept on ice and in the dark) on GF/F glass fibre filters (25 mm diameter, Whatman,
312 Cytiva, Marlborough, USA) using a vacuum pump (max. 200 mbar), until filters showed clear colouring. Samples
313 were taken for total as well as a < 20 μm fraction for better compatibility with phytoplankton community
314 measurements by flow cytometry. For the < 20 μm fraction, natural seawater was reverse sieved through a 20 μm
315 mesh before filtration onto a GF/F filter. Due to low sample volume availability at bioassay A2, the same amount
316 of water from all replicates was combined for both total and < 20 μm Chl *a* samples, resulting in one averaged
317 value for each treatment. Filters were folded once and double wrapped in aluminium foil, flash-frozen in liquid
318 nitrogen and stored at -80 °C until further analysis in the home lab. Pigments were dissolved in 90 % acetone from
319 the freeze-dried filters according to Van Leeuwe et al. (2006) and high-performance liquid chromatography
320 (HPLC) pigment separation was performed (Zobrax-Eclipse XDB-C8 column, 3.5 μm particle size) according to
321 Van Heukelem & Thomas (2001). Detection of pigments was based on both the retention time and diode array
322 spectroscopy of standards (346 nm, Waters 996), quantification was based on calibration curves using those
323 standards (DHI LAB standards). Phytoplankton community composition was determined using CHEMTAX
324 version 1.95 (Mackey et al., 1996), following Selz et al. (2018). For the final pigment ratios, see Table S6.

325

326 **2.10 Phytoplankton cell abundances (< 20 μm)**

327 Phytoplankton cell abundances were obtained using a 488 nm Argon laser benchtop Beckton-Dickinson
328 FACSCalibur (BD Biosciences, Franklin Lakes, USA) flow cytometer with the trigger set on red Chl *a*
329 autofluorescence (Marie et al., 1999). The phytoplankton samples from the Amundsen Sea bioassays were
330 measured fresh within 30 min of sampling (stored on ice); the Weddell Sea bioassay phytoplankton samples were
331 fixed for 15 – 30 min with 100 μL formaldehyde-hexamine (18 % v/v:10 % v/v) at 4 °C, flash-frozen in liquid
332 nitrogen and stored at -80 °C until analysis in the home lab. Phytoplankton populations were differentiated based
333 on their red autofluorescence and side scatter, using FCS express 5 (De Novo Software, Pasadena, CA, USA).
334 Freshly counted samples resulted in comparable gating as the fixed samples (tested for Amundsen Sea samples).



335 A total of 25 populations were distinguished (Table S7), whereby not all populations occurred in both seas and
336 all bioassays. Average cell diameters were determined by size-fractionation, i.e., serial gravity filtration through
337 20, 10, 8, 5, 3, 2, 1, 0.8 and 0.6 μm PC filters (Whatman, Cytiva, USA, Marlborough, MA) using a reusable filter
338 holder (Whatman, Cytiva, Marlborough, USA) and a plastic syringe. The number of cells retained by each filter
339 per discriminated population were plotted against the respective filter size. The average cell diameters were
340 defined as the size where 50 % of the original number of cells were retained, based on the fit of a sigmoidal plot
341 (Veldhuis & Kraay, 2004). Phyto 5, 6, 7, 11, 12 and 14 were cryptophytes that were identified by their orange
342 phycoerythrin autofluorescence. Based on earlier work (Biggs et al., 2019), we consider phytoplankton
343 populations Phyto 20 and 22 to 25 to be diatoms and Phyto 8 to be *Phaeocystis antarctica* by comparing the red
344 autofluorescence and side scatter pattern of the respective phytoplankton groups. The latter was confirmed during
345 the Amundsen Sea expedition when we selectively collected *Phaeocystis* colonies and analysed them fresh
346 onboard after gentle shaking (to break up the colonies). Phytoplankton carbon was estimated based on cell volume
347 of phytoplankton, assuming spherical cells, and using $237 \text{ fg C } \mu\text{m}^{-3}$ for picophytoplankton populations Phyto 1
348 to 6 and $196.5 \text{ fg C } \mu\text{m}^{-3}$ for nanophytoplankton populations Phyto 7 to 25 (Garrison et al., 2000; Worden et al.,
349 2004).

350

351 2.11 Statistical analyses

352 All statistical analyses were performed using R (R Core Team, 2021). To detect differences in phytoplankton
353 community composition between treatments, an ANOSIM analysis was performed (vegan library, using Bray-
354 Curtis dissimilarity with 9999 permutations). When a significant difference ($p < 0.05$) was detected, an indicator
355 species analysis (vegan library, function r.g. with 9999 permutations) was used as a follow-up analysis to see
356 which phytoplankton groups differed between treatments. This was done for both flow cytometry-based
357 abundances and pigment-based taxonomic group composition, using relative values, thus normalized against total
358 Chl *a* for pigment-based community composition, and total phytoplankton abundance for both pigment-based and
359 flow cytometry-based phytoplankton groups. For the indicator species analysis, p-values are reported. A Scheirer-
360 Ray-Hare test (non-parametric ANOVA-like test) was performed to determine the significance of Fe-addition and
361 temperature increase, as well as potential interaction effects, on the respective response variable measured. The
362 test was performed for data of the last day of the incubation, since effects were usually strongest then, and some
363 variables were only sampled at the beginning and the end of the experiment (day 6 for A1 and A2, day 8 for W1
364 and W2). We manually calculated eta-squared (η^2 , amount of variance explained, the higher the value, the larger



365 the effect) by dividing the sum of squares of the effect of interest (i.e. iron addition, temperature increase and the
366 interaction between these two) by the total sum of squares. The η^2 is provided when temperature increase, iron
367 addition, and/or the interaction between both tested as significant. Since we wanted to look at the overall effect of
368 Fe addition, temperature increase, and potential interaction effects on total phytoplankton abundances based on
369 flow cytometry, we additionally performed a generalized linear model (GLM), assuming a quasi-poisson
370 distribution in combination with a log-link, including the bioassay as well as the day number as factors without
371 interaction, and including an interaction term for the Fe- and temperature-treatment. For the GLM, the data of all
372 bioassays and all timepoints (excluding day 0) were combined. The formula for the GLM was: total phytoplankton
373 abundances ~ Fe treatment * temperature treatment + bioassay name + day number. Statistical results are only
374 reported for variables where more than 1 replicate was available. We also performed an NMDS analysis based on
375 phytoplankton abundances using the vegan library with Bray-Curtis dissimilarity (seed set to 123). A significance
376 level of $p < 0.05$ was used. Where applicable, the mean \pm standard deviation is reported, unless stated otherwise.

377

378 3. Results

379 3.1 Nutrient dynamics

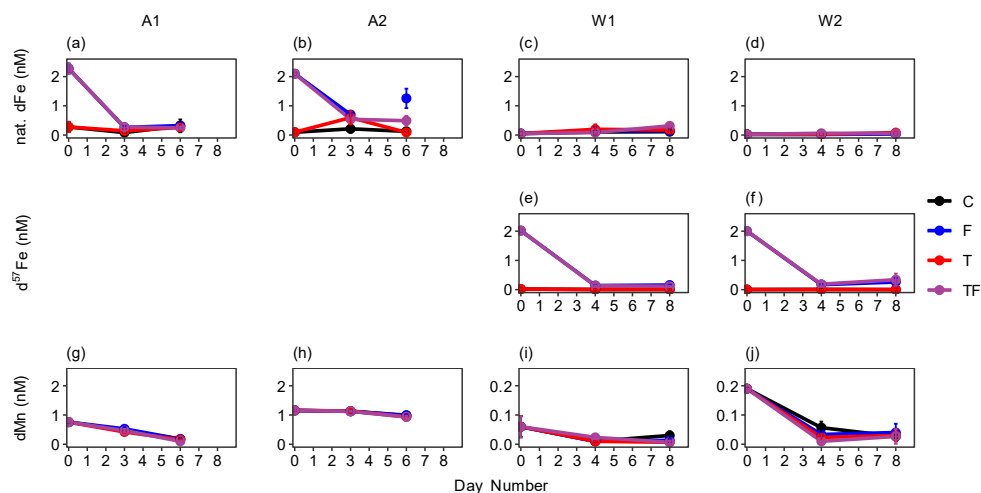
380 Bioassay treatments without Fe addition (C and T) started at naturally low dFe concentrations (0.28 ± 0.16 , 0.10
381 ± 0.02 , 0.05 ± 0.03 and 0.03 ± 0.01 nM natural dFe for bioassay A1, A2, W1 and W2, respectively), and stayed
382 within these ranges. The Fe addition treatments (F and TF) showed a rapid (and overall comparable) drawdown
383 of the added Fe (natural Fe for A1 and A2; Fig 2a, b and $d^{57}\text{Fe}$ for W1 and W2; Fig. 2e, f) in all bioassays,
384 regardless of its isotopic composition. The dFe concentrations in F and TF treatments (0.29 ± 0.07 nM) at the end
385 of the bioassays were comparable to concentrations in non-Fe addition treatments (0.28 ± 0.14 nM) for the
386 relatively high-Chl *a* bioassay A1. In contrast, bioassay A2 had most dFe left at the end of the incubation ($0.80 \pm$
387 0.46 nM for F and TF, compared to 0.11 ± 0.04 nM for C and T) which concurs with the low starting Chl *a*
388 concentration and irradiance intensity. However, since the average dFe concentration in Fe amended treatments
389 was lower (0.65 ± 0.10 nM) in the middle of the incubation period (day 3, see Figure 2 b), we cannot rule out
390 potential contamination during sampling as a reason for the higher dFe concentrations, notably in the F treatment.
391 For the Weddell Sea bioassays, $d^{57}\text{Fe}$ in F and TF treatments declined rapidly with low final concentrations (0.14
392 ± 0.03 and 0.31 ± 0.17 nM for W1 and W2, respectively) compared to the non-Fe addition treatments (0.01 ± 0.01
393 nM $d^{57}\text{Fe}$ and below detection limit for W1 and W2, respectively). Other trace metals were also measured, and
394 dissolved manganese (dMn) drawdown did not differ between treatments (Fig. 2g-j). However, the starting



395 concentrations of dMn were low for W1 and W2 (0.06 ± 0.03 and 0.19 , $SD < 0.01$ nM, compared to 0.76 , $SD <$
396 0.01 1.16 ± 0.01 nM for A1 and A2, respectively).

397 The dissolved inorganic macronutrients were not limiting phytoplankton growth during the bioassays. Final
398 concentrations were at least 7.2 , 0.3 and 37 μM in all bioassays for nitrogen, phosphate, and silicate, respectively
399 (Supplement Fig. S2). Still, there was discernible drawdown of macronutrients by the microbial community during
400 the incubations, except for Amundsen Sea bioassay A2. Fe addition (both F and TF treatments) had a significant
401 impact on phosphorous drawdown for bioassays A1, W1 and W2 ($p < 0.05$, η^2 : 0.53 , 0.76 and 0.76 for A1, W1
402 and W2, respectively; and on average 0.45 μM lower for Fe addition treatments compared to C) and on nitrogen
403 drawdown for bioassays W1 and W2 ($p < 0.004$, $\eta^2 > 0.75$, average of 9.8 μM lower for Fe addition treatments
404 compared to C). The TF treatment showed stronger drawdowns especially for Weddell Sea bioassays W1 and W2
405 (average 0.7 -fold change between TF and F treatments for both phosphorus and nitrogen, respectively), however
406 there was no significant interaction effect between temperature increase and Fe addition. In contrast, silicate acid
407 concentrations at the end of the incubation period were impacted by the increase in temperature for bioassays A1,
408 A2 and W2 ($p < 0.02$, η^2 : 0.76 for A1 and W2 and η^2 : 0.52 for A2 and $p = 0.06$ and η^2 : 0.32 for bioassay W1),
409 with T treatments showing on average a 2.4 μM lower silicate concentration compared to the control. Only
410 bioassay W1 showed an effect of Fe-addition on silicate drawdown ($p = 0.02$, η^2 : 0.52), resulting in the TF
411 treatment showing lowest concentrations on the last day of the incubations (0.8 -fold change compared to the
412 control and 0.9 -fold change compared to both T and F treatment). The ratios of silicate drawdown to nitrogen and
413 to phosphorus were higher in W1 than in W2 (i.e., 1.4 and 18.3 in W1 and 0.7 and 10.5 in W2). Moreover, when
414 Fe was added, the silicate to nitrogen ratio (Si:N), as well as silicate to phosphorous ratio (Si:P) drawdown was
415 lower in bioassays A1, W1 and W2 compared to non-Fe treatments (0.86 and 1.02 Si:N for Fe and non-Fe
416 treatments and 11.3 and 12.5 Si:P, respectively).

417



418

419 **Figure 2:** Average concentrations of natural dissolved Fe (a, b, c, d), $d^{57}\text{Fe}$ (e, f) and $d\text{Mn}$ (g, h, i, j) concentrations for
 420 Amundsen Sea (A1: a, g; A2: b, h) and Weddell Sea (W1: c, e, i; W2: d, f, g) bioassays. Amundsen Sea bioassays did not
 421 receive ^{57}Fe supplementation. The black line represents the control (C) treatment, the red line the temperature (T) treatment,
 422 the blue line the iron (F) treatment, and the purple line the combined temperature and iron treatment (TF). Error bars
 423 indicates the standard deviation ($n = 2$ or 3 , except for $d\text{Fe}$ of bioassay A2 TF treatment day 3, when they are not visible it is
 424 smaller than the symbol. Bioassay A2 showed a higher $d\text{Fe}$ concentration on day 6 compared to day 3, which we cannot
 425 exclude to be due to potential contamination and was thus treated as an outlier.

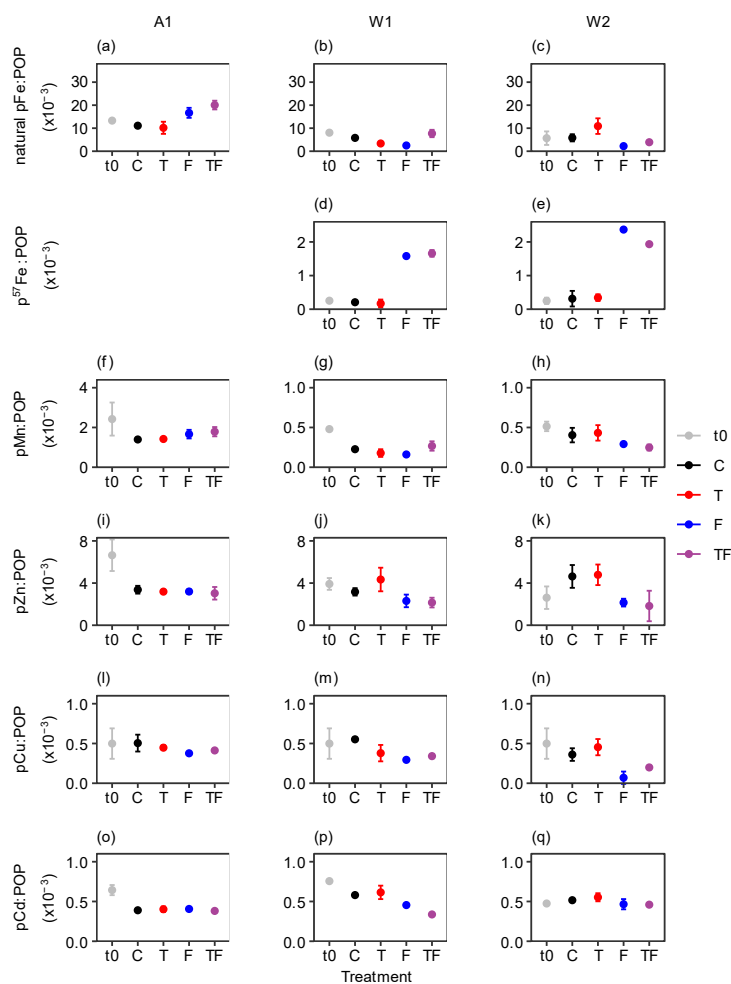
426

427 Particulate Fe concentrations (natural pFe for A1, $p^{57}\text{Fe}$ for W1 and W2) increased over time for the Fe addition
 428 treatments (Table S8) in all bioassays examined (excluding A2 as particulate metals were not measured there),
 429 and pFe concentrations at the last day of incubations were (positively) impacted by Fe-addition ($p \leq 0.01$, $\eta^2 \geq$
 430 0.73 for A1, W1 and W2, final concentrations were 8.01 ± 0.83 , 1.09 ± 0.10 , 0.89 ± 0.33 nM for Fe addition
 431 treatments and 4.40 ± 0.21 , 0.08 ± 0.02 , 0.09 , $\text{SD} < 0.01$ nM for treatments without Fe addition for A1, W1 and
 432 W2, respectively).

433 To examine potential differences in phytoplankton trace metal stoichiometry in response to Fe addition and/or
 434 warming, we calculated the ratio of pFe and other trace metals (pMn, pZn, pCd and pCu) to POP concentrations
 435 (Fig. 3, Table S8). Fe-addition significantly increased pFe:POP ratios (natural pFe for A1 and $p^{57}\text{Fe}$ for W1, W2)
 436 for all bioassays ($p \leq 0.01$, $\eta^2 \geq 0.73$; average 2.5-fold change for natural pFe:POP (A1) and 13.3-fold change for
 437 $p^{57}\text{Fe}$:POP in Weddell Sea bioassays for Fe-addition treatments compared to the control). Furthermore, the
 438 pMn:POP ratios increased (by 0.33 compared to C) due to Fe-addition in bioassay A1 and decreased (by 0.13
 439 compared to C) in W2 ($p < 0.01$ and 0.004 , η^2 : 0.74 and 0.76, respectively). For bioassay W1, neither Fe nor
 440 temperature alone had a significant impact on the pMn:POP ratio, however, the combination of both treatments
 441 tested significant ($p = 0.01$, η^2 : 0.63), with the TF treatment showing an average 1.4-fold changed ratio compared
 442 to all other treatments. Also, the pCd:POP ratio was significantly affected by Fe-addition in W1 and W2 ($p < 0.05$,



443 η_2 : 0.76 and 0.39 for W1 and W2), showing decreased values (by on average 0.12) for Fe-addition treatments
 444 compared to the control (Fig. 3 o-q), however no effect was seen for bioassay A1. A similar outcome was observed
 445 for pZn:POP ratios ($p \leq 0.01$, η_2 : 0.65 and 0.76 for W1 and W2, respectively, by on average 1.8 compared to C).
 446 For pCu:POP ratios, a decrease due to Fe-addition was mainly observed in bioassay A1 and W2 ($p < 0.009$, $\eta_2 \geq$
 447 0.73, by on average 0.16 compared to C), while for bioassay W1, Fe-addition caused a notable, but not statistically
 448 significant effect ($p = 0.09$, η_2 : 0.32, Fig. 3, by on average 0.23 compared to C).



449

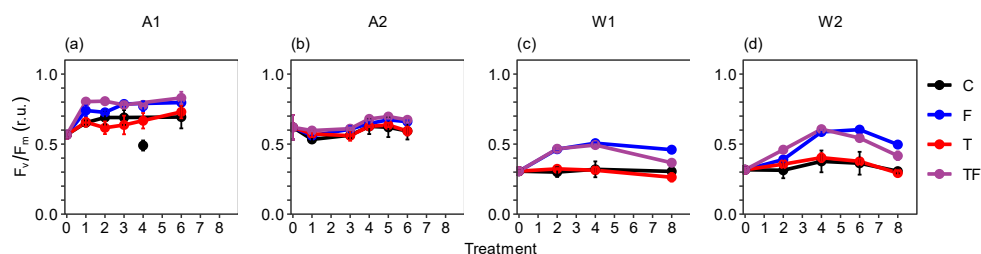
450 **Figure 3:** Average ratios ($\times 10^{-3}$, mM:M) of particulate trace metal to particulate organic phosphorus (POP) for Amundsen
 451 Sea A1 (a, f, i, l, o) and Weddell Sea W1 (b, d, g, j, m, p) and W2 (c, e, h, k, n, q) bioassays. There is no data available for
 452 A2. pFe = natural particulate, p⁵⁷Fe = particulate iron in the ⁵⁷Fe form (not added to Bioassay A1), pMn = particulate
 453 Manganese, pZn = particulate Zinc, pCu = particulate copper, pCd = particulate cadmium. t0 are starting ratios, whilst ratios
 454 for C (control), T (temperature), F (iron) and TF (combination of temperature and iron) were measured on the last day of the
 455 incubations (day 6 and 8 for Amundsen and Weddell Sea bioassays, respectively). Error bars indicates the standard deviation
 456 ($n = 2$ or 3), except for bioassay A1, T-treatment for all ratios and bioassay W1 C treatment for the pFe:POP ratio, there $n =$
 457 1. If the error bar is not visible, then it is smaller than the symbol. Please note the different y-axis ranges for manganese to
 458 POP ratios (f-h).



459 3.2 Photosynthetic efficiency

460 The photosynthetic efficiency F_v/F_m at the start of the incubations was 2-fold lower for the Weddell Sea bioassays
 461 compared to the Amundsen Sea bioassays (i.e., 0.3 vs 0.6 r.u., respectively). Fe addition led to an increase of
 462 F_v/F_m for all bioassays (Fig. 4, $p \leq 0.009$; $\eta^2 > 0.68$ for all bioassays), with stronger increases in Weddell Sea
 463 compared to Amundsen Sea bioassays (average of 1.42- and 1.14-fold change for Fe addition (F and TF) versus
 464 control treatments for Weddell and Amundsen Sea bioassays, respectively). Towards the end of the incubations
 465 of W1 and W2, F_v/F_m decreased slightly again for the Fe addition treatments (most so for TF, with final F_v/F_m
 466 values being still higher than for C and T treatments), coinciding with Fe depletion (Fig. 2).

467



468

469 **Figure 4:** Temporal dynamics of the photosynthetic efficiency (F_v/F_m , relative units) of the phytoplankton for the Amundsen
 470 Sea A1 (A), A2 (B) and the Weddell Sea W1 (C) and W2 (D) bioassays. The black line represents the control (C) treatment,
 471 the red line the temperature (T) treatment, the blue line the iron (F) treatment, and the purple line the combined temperature
 472 and iron (TF) treatment. Averages of triplicates with error bars representing the standard deviation; if not visible it is smaller
 473 than the symbol. The control treatment of bioassay A1 showed an outlier for F_v/F_m values on day 4, which was excluded.

474

475 3.3 POC, Chl *a*, and phytoplankton taxonomic community composition

476 Total Chl *a* concentration at the start of the incubations (Table 1) was highest for the ASP bioassay A1 ($3 \mu\text{g L}^{-1}$)
 477 and lowest for bioassay A2 outside the ASP ($0.4 \mu\text{g L}^{-1}$). Of the Weddell Sea bioassays, W1 had the highest Chl
 478 *a* starting concentration (1.5 compared to $0.6 \mu\text{g L}^{-1}$ for W1 and W2). Starting concentrations of total POC in A1
 479 and W1 were higher than A2 and W2 (384 and $347 \mu\text{g L}^{-1}$ compared to 91 and $136 \mu\text{g L}^{-1}$, respectively). The POC
 480 to Chl *a* ratio was lower for A1 (130) than the other bioassays (212-239). Total POC concentrations did not display
 481 differences between treatments at the end of the incubations for A1 and A2 (Fig. 5a-d), yet total Chl *a*
 482 concentrations exhibited treatment-specific differences for all bioassays (Fig. 5e-h). Fe-addition always positively
 483 impacted Chl *a* concentrations (p : 0.02, 0.005 and 0.006, η^2 : 0.52, 0.76 and 0.67 for bioassays A1, W1 and W2;
 484 not tested for A2 due to $n = 1$ for all Chl *a* samples and W1 C due to $n = 1$), however the effect was stronger in
 485 Weddell Sea Bioassays (average of 1.6- and 2.9-fold difference for Amundsen and Weddell Sea with Fe addition
 486 compared to C). Amundsen Sea bioassays also showed a slight increase in Chl *a* with increased temperatures.

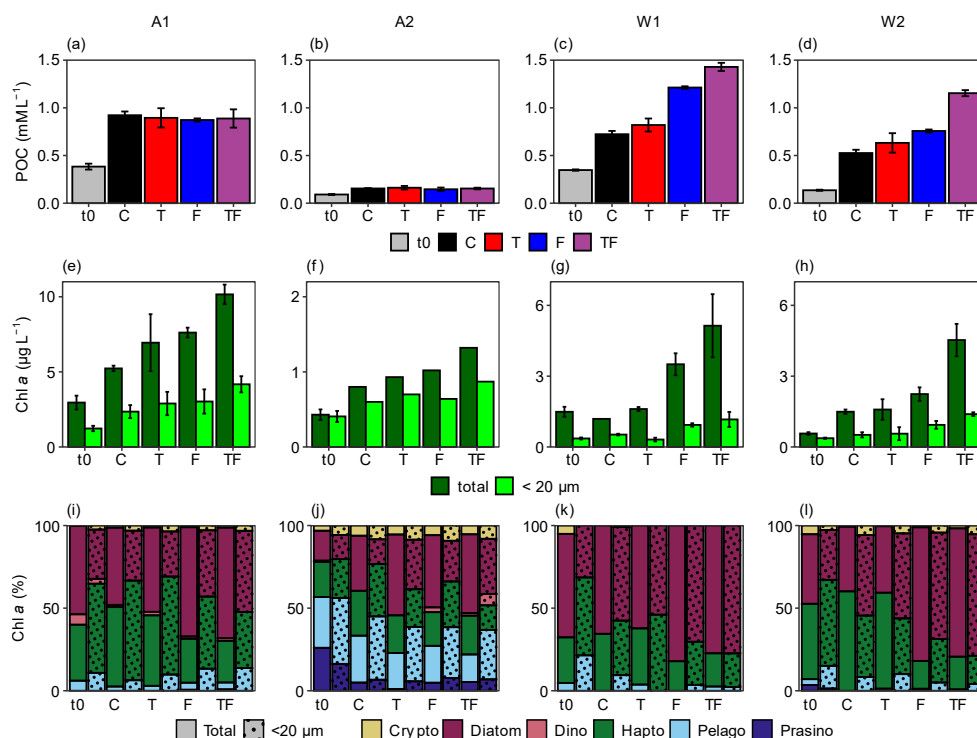


487 Strongest treatment-specific increases in Chl *a* concentrations were, however, obtained for the TF treatment in all
488 bioassays, resulting in an average of 1.7 μg more Chl *a* L^{-1} compared to the F treatment. POC concentrations in
489 W1 and W2 showed similar treatment responses as total Chl *a* in these bioassays.

490 The TF treatment also caused the strongest increase for the $< 20 \mu\text{m}$ Chl *a* fraction (Fig. 5 e–h) for all bioassays,
491 and Fe-addition generally had a positive impact on $< 20 \mu\text{m}$ Chl *a* concentrations, with effects being strongest in
492 both Weddell Sea bioassay W1 and W2 (increases of 1.2, 0.2, 0.5 and 0.7 μg L^{-1} for A1, A2, W1 and W2 compared
493 to the control, respectively and $p = 0.04$ and 0.006 , η^2 : 0.37 and 0.67. A2 and W1 were not tested due to missing
494 replicates). The $< 20 \mu\text{m}$ fraction at the start of the bioassays made up respectively 42, 24 and 65 % of total Chl *a*
495 in A1, W1 and W2, whereas for bioassay A2 95 % of the total Chl *a* concentration was $< 20 \mu\text{m}$. At the end of
496 the bioassays, shares were 42, 25, 35 % and 70 % for A1, W1, W2 and A2, respectively.

497 Diatoms dominated the phytoplankton community at the start of A1 and W1 (53 and 62 % of total Chl *a*), followed
498 by haptophytes (34 and 27 %; Fig. 5i-l). Bioassay W2 had a comparable share of diatoms and haptophytes (42
499 and 46 % of total Chl *a*), whilst the phytoplankton community of A2 was taxonomically most diverse.

500 Diatoms showed in general a strong response to Fe addition (F and TF treatment) and could be defined as an
501 indicator group for Fe addition treatments in A1 and W2 ($p < 0.005$). Absolute diatom abundances increased as
502 well with Fe-addition, especially for the TF treatment, in bioassays A1 (F and TF treatment, $p = 0.007$) and W2
503 (TF treatment, $p = 0.02$, Table S8). In bioassay W2, diatoms also showed a higher share for Fe addition treatments
504 in the $< 20 \mu\text{m}$ fraction ($p < 0.05$), with absolute abundances being higher in the TF treatment for bioassays A1,
505 W1 and W2 ($p < 0.04$), and bioassay W1 also showing higher abundances at the F treatment ($p = 0.04$). The
506 contribution of haptophytes declined (in response to the diatom increase, also in W1 where the diatom response
507 was not significant, $p < 0.007$), however their absolute concentration (in μg Chl *a* L^{-1} ; Table S8) did not decline
508 except for the F-treatment in bioassay W2 ($p = 0.01$). Both the share ($p = 0.01$) and absolute concentration ($p =$
509 0.04) of pelagophytes increased with Fe addition in the $< 20 \mu\text{m}$ fraction of bioassay A1. Cryptophyte abundances
510 increased in the total fraction of the TF treatment for A1 and W2 ($p = 0.02$ and 0.01 , respectively), and the < 20
511 μm fraction in W1 ($p = 0.02$), however their share did not change with treatments.



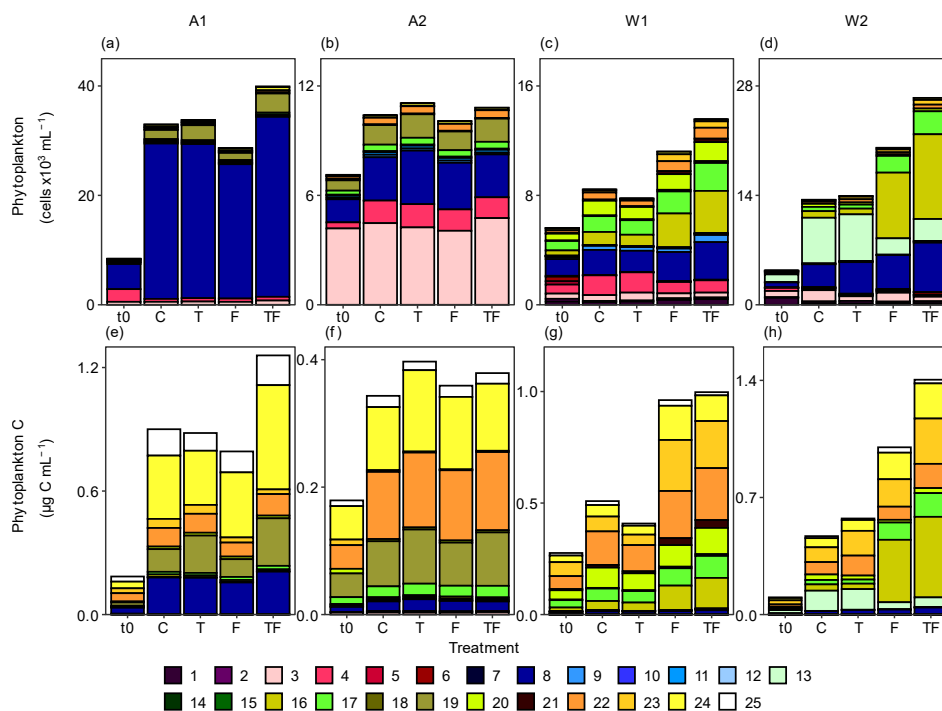
512

513 **Figure 5:** Average concentrations of particulate organic carbon (POC, a-d), total and < 20 μm (dotted columns) Chl *a* (e-h),
 514 and the taxonomic composition of the phytoplankton community (i-l, % of total Chl *a*) for the Amundsen Sea A1 (a, e, i)
 515 and A2 (b, f, j), and the Weddell Sea W1 (c, g, k) and W2 (d, h, l) bioassays. Error bars represent the standard deviation ($n =$
 516 3 except when no error bar is shown, then $n = 1$). t0 = starting conditions, C = control, T = temperature treatment, F = iron
 517 addition treatment, TF = temperature and iron addition treatment. For i-l, Crypto, Dino, Hapto, Pelago and Chloro stands for
 518 cryptophytes, dinophytes, haptophytes, pelagophytes and chlorophytes, respectively. Solid bars represent the total and
 519 shaded bars the < 20 μm fraction community composition. Note the difference in y-axis for the Chl *a* panels e-h.

520

521 3.4 Phytoplankton abundances

522 The total abundances of < 20 μm phytoplankton (Fig. 6, Fig. S3, Table S8) increased with time for all bioassays
 523 and the treatment-specific dynamics largely mimicked the responses observed for the < 20 μm Chl *a* fraction (Fig.
 524 5e-h). Bioassay A1 had overall the highest phytoplankton abundances (up to $40,000 \pm 4,000$ cells mL^{-1} for the TF
 525 treatment; Fig. 6a) and was dominated by *Phaeocystis antarctica* Phyto 8 (highest abundances of $37,053 \text{ mL}^{-1}$
 526 were observed in the TF treatment; Table S8). Phyto 19 increased specifically in abundance and share (Fig. 6a) in
 527 the temperature treatments ($2,800$ and $3,500$ cells mL^{-1} for T and TF, compared to $1,700$ and $1,300 \text{ mL}^{-1}$ for C and
 528 F, $p < 0.01$). Phyto 24 was positively impacted by the TF treatment, i.e., 361 vs 595 cells mL^{-1} for C and TF
 529 treatment, respectively ($p < 0.05$).



530

531 **Figure 6:** Flow cytometry-based phytoplankton community composition (a-d) and carbon (e-h) at the start (t0) and the end
 532 of the bioassay incubations for the different treatments (average of triplicates) for Amundsen Sea bioassays A1 (a, e), A2 (b,
 533 f), and Weddell Sea bioassays W1 (c, g) and W2 (d, h). t0 = starting conditions, C = control, T = temperature treatment, F =
 534 iron addition treatment, TF = temperature and iron addition treatment. Phytoplankton groups are sorted by size, with Phyto 1
 535 – 6 ≤ 3 µm, Phyto 7 – 20 ≤ 10 µm and Phyto 21 – 25 ≥ 10 µm. Phyto 5, 6, 7, 11, 12 and 14 are cryptophytes, Phyto 20, 22 –
 536 25 diatoms and Phyto 8 *Phaeocystis antarctica*. Note the different scales.

537

538 When converted to cellular carbon based on cell volume using 237 and 196.5 fg C µm⁻³ as conversion factors for
 539 Pico- and Nanophytoplankton, respectively (Fig. 6e), the strong positive response of the phytoplankton to the TF
 540 treatment was mostly due to this larger-sized Phyto 24 (average diameter of 19 µm, p = 0.01, stat: 0.92) and to
 541 smaller extent Phyto 19 (p < 0.01). Bioassay A2 presented the highest share of picoeukaryotes, especially Phyto
 542 3 (59 % compared to max. 18 % in the other bioassays, Fig. 6b). No apparent treatment-specific responses were
 543 recorded, apart from Phyto 19 that increased somewhat with warming (p = 0.04). The phytoplankton populations
 544 in W1 were distributed more equally (Fig. 6c), with higher abundances of especially Phyto 16 and 17 for the Fe
 545 addition treatments (p < 0.05, most pronounced for TF with average abundances of 3,103 ± 1,290 vs 948 ± 218
 546 cells mL⁻¹ and 2,041 ± 572 vs 1,158 ± 216 cells mL⁻¹ for Phyto 16 and 17 in the TF vs C treatments, respectively).
 547 When expressed in carbon, Phyto 16 was still a recognisable indicator species (p = 0.03) but at the same time the
 548 larger-sized Phyto 21 (average cell diameter of 10 µm) and diatoms Phyto 22-24 (13-19 µm) showed clear positive
 549 responses to Fe addition (Fig. 6g, p < 0.05 for all). Bioassay W2 also showed a distinct shift in favour of Phyto



550 16 and Phyto 17 (away from Phyto 13), already early in time (Table S8), both for abundances and cellular carbon
551 (Fig. 16d, h, $p < 0.01$ for all). Diatom 24 responded positively to Fe addition (F and TF, Fig. 16h, $p < 0.01$), similar
552 as for bioassay W1, and diatom Phyto 23 showed higher abundances for the TF treatment ($p = 0.04$). Phyto 19
553 was the only phytoplankton population that showed a consistent selective positive response (in share) to warming
554 (and not to Fe addition) in the Amundsen Sea bioassays. Diatom Phyto 22 increased with temperature in bioassay
555 W2 ($p \leq 0.01$). We refer to Table S8 for less pronounced responses of the other phytoplankton populations.
556 Overall, the response by the larger phytoplankton populations is also illustrated by the higher average cellular
557 biovolumes in the F and TF treatments of W1 and W2 (Fig. S4). The Amundsen Sea bioassays did not show a
558 treatment-specific increase in phytoplankton biovolume. Fe-addition had a significant effect on total
559 phytoplankton abundances for Weddell Sea bioassays ($p < 0.02$, η^2 : 0.96 and 0.74 for W1 and W2, with Fe addition
560 leading to an average 1.6-fold change compared to C). The GLM we performed (explained deviance: 86 %),
561 indicates an interaction effect of Fe-addition and warming ($p = 0.03$ for the interaction, exponentiated coefficient
562 (ec): 1.13), i.e. Fe-addition of 2 nM in combination with a 2 °C temperature increase led to an overall increase in
563 algal abundances of about 28 %. Fe-addition (ec: 1.03), temperature increase (ec: 1.11), bioassay and day number
564 ($p < 0.001$ for all, for other statistical parameters, see Table S9) were also significant explanatory factors. The
565 NMDS analysis of the Weddell Sea bioassays (Fig. S5c, d) demonstrated clear distinction between the Fe addition
566 treatments and the non-addition treatments after the second day of the incubations. For bioassay W1, the TF and
567 T treatments clustered on the last day of incubation separately from the F and C treatments, respectively. For
568 bioassay W2, the T treatment also separated on the last day while the TF and F treatments remained closer
569 together. Bioassays A1 and A2 did not display obvious clustering by treatment, other than time (i.e., separation
570 after day 2).

571

572 **4. Discussion**

573 **4.1 Trace metal and macronutrient dynamics**

574 The pFe concentrations showed the expected significant increase in the Fe addition treatments for both Amundsen
575 (natural dFe added) and the Weddell Sea bioassays ($d^{57}\text{Fe}$ added) at both temperatures, indicating that the added
576 dFe was indeed taken up and incorporated in the phytoplankton cells. Additionally, in bioassay W2 the final $p^{57}\text{Fe}$
577 in the TF treatment was higher than in the F treatment (1.12 ± 0.11 nM compared to 0.66 ± 0.20 nM),
578 demonstrating enhanced Fe uptake with higher temperatures. The higher starting concentrations of dFe in the
579 Amundsen Sea, compared to the Weddell Sea, can be attributed to the Fe input from basal melt (Rignot et al.,



580 2013). Conversely, the naturally low dFe concentrations in the Weddell Sea underscore the area's limited Fe input
581 (e.g. de Baar et al., 1990; Klunder et al., 2012).

582 Fe is needed in nitrate assimilation and as such uptake of nitrate is coupled to the Fe nutritional status (Schoffman
583 et al., 2016). Similarly, diatom cellular silicate to nitrogen ratios are known to increase in response to Fe stress
584 (Meyerink et al., 2017). Highest drawdown of the macronutrients typically occurred in the TF treatment, which
585 also showed the largest phytoplankton accumulation. However, whilst dissolved inorganic phosphate and nitrogen
586 drawdown was mostly affected by Fe addition, silicate drawdown in bioassays A1 and W2 was more impacted by
587 temperature. Despite a lower Chl *a* concentration (both total and < 20 µm) and phytoplankton abundance for the
588 T than the TF treatment in these bioassays, the silicate drawdown was comparable. Although Fe stress is reported
589 to cause reduced cellular Chl *a* concentrations compared to Fe replete conditions (Greene et al., 1992), it is an
590 unlikely cause as the total phytoplankton abundances displayed similar differences between the T and TF
591 treatment compared to < 20 µm Chl *a* concentrations. Instead, higher temperature may have stimulated Si uptake,
592 as reported for the diatom *Pseudonitzschia seriata* at temperatures above 0 °C (Stapleford & Smith, 1996). It
593 might also be that the T treatment experienced higher Fe stress than the control, which is also known to increase
594 Si uptake (Meyerink et al., 2017). However, since phytoplankton abundances and Chl *a* concentrations were not
595 higher in T treatments compared to the control, and since phytoplankton requires less Fe at higher temperatures
596 (Jabre & Bertrand, 2020), this is less likely. Bioassay W1 showed the strongest decline in silicate concentrations,
597 with both temperature and Fe affecting silicate drawdown. The relatively high fraction of diatoms (and specifically
598 the large-sized Phyto 20 and 22-24) in bioassay W1 could theoretically have caused the strong silicate drawdown
599 and high ratio of silicate relative to nitrogen (or phosphorus) uptake for all treatments. However, A1 also had high
600 diatom abundances and over the course of the incubations the concentration of diatoms in W2 became comparable
601 to W1. An alternative explanation may be that Mn stress in W1 (0.06 ± 0.04 vs 0.19 ± 0 nM in W1 and W2,
602 respectively) enhanced Si uptake, similar to Fe stress (Hutchins & Bruland, 1998). Increased Si uptake by diatoms
603 under a combined Fe and Mn limitation may possibly enhance protection against grazers (Assmy et al., 2013;
604 Ryderheim et al., 2022) and/or enhance sinking to more nutrient-rich depths (Waite & Nodder, 2001). Considering
605 an increasing awareness of trace metal co-limitation of phytoplankton growth (Wu et al., 2019; Browning et al.,
606 2021; Balaguer et al., 2022; Burns et al., 2023), we recommend further investigation into these potential
607 interactions and their ecological relevance.

608 Dissolved Mn is known to (co-)limit Southern Ocean phytoplankton growth and community composition
609 (Balaguer et al., 2022). Although Fe addition (F and TF treatments) led to 1.8 (0.11 ± 0.03 vs 0.06 ± 0.02 d⁻¹) and



610 1.5-fold (0.23 ± 0.02 vs 0.15 ± 0.01 d⁻¹) higher net growth rates (based on total phytoplankton abundances) in W1
611 and W2 compared to the control. The lower starting concentrations of dMn in W1 compared to W2 may have
612 contributed to the 2-fold lower phytoplankton net growth rates in W1 compared to W2, independent of the
613 treatment. Since Fe addition still led to an increased growth rate even with low dMn concentrations, Fe must have
614 been the main limiting factor.

615

616 **4.2 Micronutrient stoichiometry**

617 The observed pFe:POP ratios increased upon the addition of iron (natural pFe for bioassay A1 and p⁵⁷Fe for
618 bioassays W1 and W2), validating the experimental design and confirming the uptake of added dFe by
619 phytoplankton. For other bio-essential (Mn, Zn, Cu) or bio-active (Cd) metals, the metal:POP ratio is expected to
620 be elevated under Fe stress due to upregulation of non-specific divalent metal transporters under Fe stress (e.g.
621 Kustka et al., 2007; Lane et al., 2008) or the increased uptake of phosphorous relative to metals under Fe replete
622 conditions (growth-dilution; Cullen et al., 2003). Specifically for Mn, this might also be due to a higher cellular
623 Mn requirement under Fe stress (Peers & Price, 2004). The pMn:POP ratios were indeed higher in the C and T
624 treatments compared to the F and TF treatments of W2, but for W1, no consistent effect of Fe was observed (Fig.
625 3).

626 In contrast, slightly elevated pMn:POP ratios were observed after Fe addition in A1 (F and TF treatments),
627 matching findings by McCain et al. (2021) and Hawco et al. (2022), showing increased Mn demand in
628 environments with high Fe concentrations. Such variation likely reflects adaptive changes in nutrient uptake and
629 storage mechanisms under nutrient stress but could also be due to different phytoplankton community
630 compositions and/or environmental conditions. For example, Twining et al. (2004) observed elevated pMn:POP
631 ratios in individual diatom cells under iron deplete conditions, relative to iron replete conditions, whereas the trend
632 was opposite for autotrophic flagellated cells. However, diatoms were dominant in the F and TF treatments in all
633 experiments, suggesting that other factors besides differences in community composition play a role. The starting
634 dMn concentrations differed between the bioassays, whereby the high starting concentrations of dMn in A1 could
635 potentially explain the increased pMn:POP ratios in the F and TF treatments of this experiment., We speculate
636 that a high availability of both Fe and Mn under the low light conditions in A1 could have led to increased Mn
637 uptake for use in photosynthesis. Since dMn levels are thought to increase with Fe input (e.g. due to ice shelf
638 melting; Van Manen et al., 2022), we recommend including dMn in future studies examining the effects of global
639 climate change on phytoplankton growth.



640 Besides Mn, other trace metals are known to have variable ratios with respect to POP under different
641 environmental conditions. For example, cellular Cu requirements increase under Fe limitation (Schoffman et al.,
642 2016), which could explain the higher pCu:POP ratios in the C and T treatments compared to the Fe addition
643 treatments (Fig. 3). Similarly, the pZn:POP ratios were also elevated in the non-Fe treatments in W1 and W2, akin
644 to the pCd:POP ratios especially in W1, suggesting higher uptake of metals under Fe limitation as previously
645 suggested (Cunningham & John, 2017). Future studies linking these stoichiometric ratios with molecular
646 measurements (e.g. protein expression patterns) could provide further insight into the processes which underpin
647 trace metal uptake and use within phytoplankton communities under change. Nevertheless, this study highlights
648 a potential trend of increased uptake of essential and non-essential metals (specifically zinc, copper and cadmium)
649 by phytoplankton under Fe-deplete conditions. This trend underscores the adaptive strategies employed by
650 phytoplankton in navigating nutrient scarcities, emphasizing the complexity of nutrient interactions and their
651 collective impact on phytoplankton ecology under varying environmental conditions (e.g. Cunningham and John,
652 2017). Due to the importance of nutrient uptake in the Southern Ocean for the stoichiometry of global nutrient
653 distributions, notably at lower latitudes (Sarmiento et al., 2004; Middag et al., 2020), changes in (micro-)nutrient
654 consumption in the Southern Ocean can have global ramifications for both productivity and ecosystem structure
655 (Moore et al., 2018) which should be further explored in future (modelling) studies.

656

657 **4.3 Impact of Iron and Temperature on Phytoplankton Dynamics**

658 The Weddell Sea bioassays exhibited stronger Chl *a* accumulation and increased phytoplankton abundances in
659 response to Fe addition than the Amundsen Sea bioassays, which is likely due to the lower dFe concentrations
660 (and hence higher degree of Fe limitation for the phytoplankton typical for the Weddell Sea) at the start of the
661 incubations. While for the Weddell Sea bioassays the POC concentrations followed comparable responses to total
662 Chl *a* upon Fe addition (Fig. 5), the POC concentrations in the Amundsen Sea bioassays did not. The lower
663 irradiance during the incubations of A1 and A2 most likely led to the higher Chl *a*:POC ratios at the end of
664 incubations (i.e., average over all treatments 0.008 ± 0.002 and 0.003 ± 0.003 for the Amundsen and Weddell Sea
665 bioassays). Enhanced Chl *a*:POC ratios are a known acclimation to low light (Laws & Bannister, 1980; Geider,
666 1987; Geider et al., 1998; Wang et al., 2009). Despite the low light intensities, Chl *a* concentrations and
667 phytoplankton abundances in the control treatment increased over time in the Amundsen Sea bioassays (especially
668 in A1, net growth rate based on abundances of 0.23 ± 0.02 d⁻¹), which indicates that the phytoplankton
669 communities were low light adapted. Low light conditions are common for Amundsen Sea phytoplankton



670 (Schofield et al., 2015; Park et al., 2017) but still, the very low irradiance in A2 seemed to have limited growth
671 ($0.09 \pm 0.01 \text{ d}^{-1}$) as also illustrated by incomplete depletion of the dFe added (after 6 days of incubation). Although
672 earlier studies reported positive responses of phytoplankton to Fe addition also under low light conditions (Viljoen
673 et al., 2018; Alderkamp et al., 2019), the light intensities used for the low light treatment in those studies were
674 relatively high (i.e., 15 and 30 $\mu\text{mol quanta m}^{-2} \text{ s}^{-1}$) and well above those in A1 and A2 (average of 3.4 and 1.5
675 $\mu\text{mol quanta m}^{-2} \text{ s}^{-1}$). Considering diatoms being the taxonomic group responding strongest to Fe additions (Noiri
676 et al., 2005; Feng et al., 2010; Hinz et al., 2012; Mills et al., 2012; Zhu et al., 2016), the low proportion of diatoms
677 at the start of A2 may also have delayed a measurable effect of Fe addition. Since both Weddell Sea and Amundsen
678 Sea bioassays were initiated at times corresponding to the peak phytoplankton growth periods in each region, it is
679 unlikely that the sampling time had a major effect on our results.

680 Consistent with the lower dFe concentrations was the reduced *in-situ* F_v/F_m of the phytoplankton in W1 and W2
681 compared to Amundsen Sea bioassays, which stayed low for non-Fe addition treatments throughout the
682 experiments. Although we cannot exclude that the lower light availability in A1 and A2 may have caused
683 enhanced F_v/F_m (compared to W1 and W2; From et al., 2014), low F_v/F_m is a common indicator of Fe stress in the
684 Southern Ocean (Greene et al., 1992; Olson et al., 2000; Mills et al., 2012; Jabre and Bertrand, 2020). In addition,
685 the low dMn concentration at the start of bioassay W1 may have contributed to the low F_v/F_m (Wu et al., 2019).
686 Nevertheless, Fe addition also had a positive effect on F_v/F_m in Amundsen Sea bioassays, matching earlier reports
687 that F_v/F_m of ASP phytoplankton is partly controlled by Fe (Alderkamp et al., 2015). The decrease in F_v/F_m in the
688 F and TF treatments towards the end of the Weddell Sea bioassays might indicate that added Fe depleted towards
689 potentially limiting conditions or might be an indication of Mn (co-)limitation.

690

691 **4.4 Enhanced responses to Fe with warming**

692 Fe addition led to an overall positive response of Chl *a* concentrations, phytoplankton photophysiology and
693 growth, but more so when combined with the ecologically relevant increase in temperature. The increase in
694 phytoplankton abundances was especially distinct for Weddell Sea bioassays. GLM analysis revealed that
695 temperature alone was a significant factor for total phytoplankton abundances, however more specifically, only
696 Phyto 19 and Phyto 22 abundances displayed significant positive responses to temperature alone (T treatment).
697 The 2 °C warming alone was thus not a major driver of phytoplankton net growth in our bioassays, but accelerated
698 and enhanced Fe-addition responses (significant interaction effect for iron addition and temperature increase on
699 total phytoplankton abundances). The enhanced response to Fe with temperature was especially distinct for



700 bioassay W2 (average 1.61-fold change in the TF treatment compared to both F and T treatments). Despite low
701 light levels, this was also seen in Amundsen Sea bioassay A1, albeit to a lower extent (average 1.29-fold change
702 in the TF treatment compared to both F and T treatments). Larger-sized ($> 20 \mu\text{m}$) diatoms were mainly
703 responsible for the Chl *a* accumulation, which is consistent with previous studies (Noiri et al., 2005; Feng et al.,
704 2010; Hinz et al., 2012; Mills et al., 2012; Zhu et al., 2016) and supports the general consensus that especially
705 large phytoplankton show enhanced growth upon Fe addition due to their lower surface to volume ratio (Scharek
706 et al., 1997). But also (slightly) smaller diatoms Phyto 23 and 24 (average cell diameter of 15 and 19 μm ,
707 respectively) responded positively to the combination of Fe and temperature. Diatoms Phyto 24 was even the main
708 phytoplankton population responsible for the increase in the $< 20 \mu\text{m}$ Chl *a* fraction of the TF treatment in A1.
709 The NMDS analysis based on $< 20 \mu\text{m}$ phytoplankton abundances showed clustering for W1 and W2 driven by
710 Fe addition and temperature, indicating that also smaller-sized phytoplankton display positive responses. This is
711 supported by increased $< 20 \mu\text{m}$ Chl *a* concentrations and the 2.2 fold change in cellular carbon of $< 20 \mu\text{m}$
712 phytoplankton in F and TF treatments in the Weddell Sea bioassays (compared to the C and T treatments).
713 Specifically, we recorded distinct abundance increases of the small 7 μm Phyto 16 and Phyto 17, in the F and TF
714 treatments of W2. *Phaeocystis antarctica* (Phyto 8; 3.7 μm) also displayed higher abundances under the TF
715 treatment for W2 but the effect was not very apparent and overall, *P. antarctica* seems to handle the other
716 treatments consistently well. Rose et al. (2009) and Zhu et al. (2016) also found diatoms preferentially stimulated
717 by Fe addition and/or temperature over *P. antarctica*, which was also found in a broader context where *P.*
718 *antarctica* dominated under Fe-low conditions, whilst diatoms dominated in regions with higher Fe concentrations
719 (Arrigo et al., 2017). In contrast, Andrew et al. (2019) found comparable growth rates for *P. antarctica* and several
720 diatom cultures (tested under Fe addition and warming treatments). Similar to our study, they found highest
721 growth for the combined Fe addition and warming treatment for most species. Since diatoms tended to increase
722 strongest with Fe addition, it can be speculated that phytoplankton community compositions shift towards more
723 diatoms with increases in Fe concentrations, however other biogeochemical factors are also important to consider.
724 The positive phytoplankton growth responses were population specific and Phyto 13 (5.5. μm) in W2 even showed
725 reduced abundances for the F and TF treatments, underscoring the multifaceted factors controlling phytoplankton
726 dynamics and emphasizing the importance of understanding how trace metal concentrations and climate change
727 influence the marine ecosystems in the Southern Ocean.

728

729



730 **5. Conclusions**

731 Our study stands out that it combined chemistry and biology, Chl *a*, and population abundance to examine co-
732 effects using natural Antarctic phytoplankton communities at environmentally realistic Fe concentrations (+ 2
733 nM) and a predicted (2 °C) temperature increase (Boyd et al., 2015; Jabre et al., 2021; Andrew et al., 2022). So
734 far, studies investigating combined effects using natural Antarctic phytoplankton communities focussed on the
735 Ross Sea and tested 3 – 6 °C warming (Rose et al., 2009; Jabre et al., 2021). Our bioassays incubations were
736 performed under trace metal clean conditions (the entire duration) and with temperature remaining stable over the
737 course of incubations (maximum fluctuation of temperature \pm 0.3 °C). We stress the importance of trace metal
738 clean working conditions to avoid inadvertently assigning Fe addition effects on phytoplankton to temperature
739 when working in low Fe regions (i.e. Southern Ocean, but also open oceans in general). The differences we found
740 between the F and TF treatment may have been assigned to temperature alone under non-trace metal clean working
741 conditions (as Fe would inadvertently have been introduced), whilst our results show that temperature alone did
742 not have a (major) effect.

743 In general, the addition of Fe was the primary factor for observed stimulatory effects. In particular, large diatoms
744 benefitted from Fe addition, although several smaller-sized phytoplankton populations showed enhanced
745 abundances upon Fe addition. Given that the intensity of the observed effects varied between the experiments
746 with distinctly different phytoplankton communities, this study emphasizes the need for studying diverse regions
747 of the Southern Ocean to better understand and predict potential future changes, especially as future changes in
748 Fe availability are region-specific (Tagliabue et al., 2016; Van Manen et al., 2022). Factors such as the dFe
749 concentrations, other trace metal concentrations which may potentially co-limit phytoplankton growth, and light
750 availability, should also be considered when studying the effects of future climate on Antarctic phytoplankton.
751 Moreover, the time of the year affects the starting composition of the phytoplankton community, and the sequence
752 of the treatments in case of dual treatments (Fe addition and temperature increase) may affect the responses
753 (Brooks and Crowe 2019), hence these factors should be considered.

754 Depending on the geographical region and the time in the productive season (Thomalla et al., 2023), global
755 warming is predicted to increase wind-induced mixing or strengthen vertical stratification (Bronseleer et al., 2020;
756 De Lavergne et al., 2014; Hillenbrand & Cortese, 2006; Shi et al., 2020). Phytoplankton will bloom earlier in the
757 productive season as a result of decreasing sea ice and consequently higher light (Krumhardt et al., 2022), rapidly
758 drawing down available Fe, followed by stratification, and thus favourable conditions for smaller-sized
759 phytoplankton (Deppeler & Davidson, 2017; Krumhardt et al., 2022). Our study shows, however, that enhanced



760 Fe input in such regions may partly overturn this warming-induced shift, assuming macronutrients will not become
761 limiting.

762 Alterations in phytoplankton community composition and cell size, as observed in our experiments, will directly
763 affect top-down control by grazers and viral infection and consequently trophic transfer efficiency. Moreover, not
764 only the flow of organic carbon through the food web will be affected, but also the flux of organic carbon to
765 deeper layers of the ocean (biological carbon pump) depends on the phytoplankton community composition, cell
766 size and type of loss factor. We recommend that future bioassay studies consider phytoplankton gross growth,
767 grazing, and viral lysis as well. After all, the typically reported net changes in the bioassay phytoplankton
768 community are the resultant of production and losses. Both Fe as well as temperature can impact the extent of the
769 loss factors. For example, grazing rates are known to increase with temperature (Chen et al., 2012; Caron &
770 Hutchins, 2013), viral lysis may occur faster at higher temperature (Maat et al., 2017), and Fe availability can
771 affect algal virus production and infectivity (Slagter et al., 2016). Finally, potential region-specific differences in
772 the share of grazing and lysis (Mojica et al., 2016; Mojica et al., 2021; Eich et al., 2022) may influence net changes
773 in phytoplankton biomass or abundances in bioassays. The Southern Ocean biogeochemical cycling and
774 ecosystems dynamics are complex and need to be better studied in field and modelling studies. The current study
775 underlines the need for assessing consequences of near future temperature changes at environmentally relevant
776 dFe concentrations.

777

778 *Data availability:* All data presented in this paper (nutrients, trace metals, phytoplankton abundances,
779 photosynthetic efficiencies, Chl *a* concentrations, pigment based community composition, particulate organic
780 carbon and particulate organic phosphate) are included in this published article and are available under
781 <https://doi.org/10.25850/nioz/7b.b.hh>.

782

783 *Supplement:* The supplementary material related to this article is available online at XXX.

784

785 *Author contributions:* RM and CPDB conceptualized the study. CE, MvM, EB, SBEHP, HT, IA, JSPM and RM
786 conducted the fieldwork under the lead of RM, JJ analysed the nutrient samples for Amundsen Sea bioassays,
787 WvdP analysed the pigment samples and conducted the Chemtax analysis, CE, MvM, wrote the original draft,
788 CPDB and RM edited the paper. EB, LJ and JSPM contributed to the discussion. All authors contributed to
789 commenting on the paper.



790

791 *Competing interests:* The authors declare that they have no conflict of interest.

792

793 *Acknowledgements:* We would like to thank the captain and crew of both the R/V Araon and the R/V Polarstern,
794 as well as the expedition leaders SangHoon Lee and Olaf Boebel and all other expedition participants. Our
795 participation in R/V Polarstern expedition PS117 was funded by AWI under grant number AWI_PS117_02.
796 Furthermore, we would like to thank John Seccombe from Aquahort for his support in conceiving and building
797 the heatpumps as well as his remote support during the expeditions and Sharyn Ossebaar for nutrient
798 measurements aboard R/V Polarstern. Sven Ober and all the colleagues from NIOZ national marine facilities
799 (NMF) for the preparation of the Titan sampling system during the expeditions, as well as building the incubators
800 and their help in the expedition preparation. We are also grateful to Bob Kusters (NIOZ) for his assistance with
801 the incubators, ensuring they maintained the correct temperature throughout our study. Patrick Laan (NIOZ) for
802 helping with the ICP-MS analyses, Flora Wille (NIOZ) for helping with the particulate metal analysis and Piet ter
803 Schure and his team (DMT Marine Equipment) for supplying a winch system last minute for the Titan sampling
804 system used on the R/V Araon.

805

806 *Financial support:* This work was part of the FePhyrus project (ALWPP.2016.020), which was supported by the
807 Netherlands Polar Programme (NPP), with financial aid from the Dutch Research Council (NWO). Mathijs van
808 Manen was supported by the Utrecht University-NIOZ collaboration. The ANA-08B expedition was supported
809 by the Korea Polar Research Institute grant KOPRI PE24110. The PS117 expedition was supported by the
810 auxiliary use proposal AWI_PS117_02. EMB was supported by an NSERC Canada Research Chair.



811 **References**

- 812 Aflenzer, H., Hoffmann, L., Holmes, T., Wuttig, K., Genovese, C., & Bowie, A. R. (2023). Effect of dissolved
813 iron (II) and temperature on growth of the Southern Ocean phytoplankton species *Fragilariopsis*
814 *cylindrus* and *Phaeocystis antarctica*. *Polar Biology*, 46(11), 1163–1173.
815 <https://doi.org/10.1007/s00300-023-03191-z>
- 816 Alderkamp, A.-C., van Dijken, G. L., Lowry, K. E., Connelly, T. L., Lagerström, M., Sherrell, R. M., Haskins,
817 C., Rogalsky, E., Schofield, O., Stammerjohn, S. E., Yager, P. L., & Arrigo, K. R. (2015). Fe
818 availability drives phytoplankton photosynthesis rates during spring bloom in the Amundsen Sea
819 Polynya, Antarctica. *Elementa: Science of the Anthropocene*, 3(C), 000043.
820 <https://doi.org/10.12952/journal.elementa.000043>
- 821 Alderkamp, A.-C., Van Dijken, G. L., Lowry, K. E., Lewis, K. M., Joy-Warren, H. L., Van De Poll, W., Laan,
822 P., Gerringa, L., Delmont, T. O., Jenkins, B. D., & Arrigo, K. R. (2019). Effects of iron and light
823 availability on phytoplankton photosynthetic properties in the Ross Sea. *Marine Ecology Progress*
824 *Series*, 621, 33–50. Scopus. <https://doi.org/10.3354/meps13000>
- 825 Alfred-Wegener-Institut Helmholtz-Zentrum für Polar- und Meeresforschung. (2017). Polar Research and
826 Supply Vessel POLARSTERN Operated by the Alfred-Wegener-Institute. *Journal of large-scale*
827 *research facilities*, 3, A119. <http://dx.doi.org/10.17815/jlsrf-3-163>
- 828 Andrew, S. M., Morell, H. T., Strzepek, R. F., Boyd, P. W., & Ellwood, M. J. (2019). Iron availability
829 influences the tolerance of southern ocean phytoplankton to warming and elevated irradiance. *Frontiers*
830 *in Marine Science*, 6, 681.
- 831 Andrew, S. M., Strzepek, R. F., M. Whitney, S., Chow, W. S., & Ellwood, M. J. (2022). Divergent
832 physiological and molecular responses of light- and iron-limited Southern Ocean phytoplankton.
833 *Limnology and Oceanography Letters*, 7(2), 150–158. <https://doi.org/10.1002/lo2.10223>
- 834 Annett, A. L., Skiba, M., Henley, S. F., Venables, H. J., Meredith, M. P., Statham, P. J., & Ganeshram, R. S.
835 (2015). Comparative roles of upwelling and glacial iron sources in Ryder Bay, coastal western
836 Antarctic Peninsula. *Marine Chemistry*, 176, 21–33.
- 837 Arrigo, K. R., & van Dijken, G. L. (2003). Phytoplankton dynamics within 37 Antarctic coastal polynya
838 systems. *Journal of Geophysical Research: Oceans*, 108(8), 27-1-27–18.
839 <https://doi.org/10.1029/2002jc001739>



- 840 Arrigo, K. R., van Dijken, G. L., Alderkamp, A.-C., Erickson, Z. K., Lewis, K. M., Lowry, K. E., Joy-Warren,
841 H. L., Middag, R., Nash-Arrigo, J. E., Selz, V., & van de Poll, W. (2017). Early Spring Phytoplankton
842 Dynamics in the Western Antarctic Peninsula. *Journal of Geophysical Research: Oceans*, 122(12),
843 9350–9369. <https://doi.org/10.1002/2017JC013281>
- 844 Assmy, P., Smetacek, V., Montresor, M., Klaas, C., Henjes, J., Strass, V. H., Arrieta, J. M., Bathmann, U., Berg,
845 G. M., & Breitbarth, E. (2013). Thick-shelled, grazer-protected diatoms decouple ocean carbon and
846 silicon cycles in the iron-limited Antarctic Circumpolar Current. *Proceedings of the National Academy
847 of Sciences*, 110(51), 20633–20638.
- 848 Balaguer, J., Koch, F., Hassler, C., & Trimborn, S. (2022). Iron and manganese co-limit the growth of two
849 phytoplankton groups dominant at two locations of the Drake Passage. *Communications Biology*, 5(1),
850 Article 1. <https://doi.org/10.1038/s42003-022-03148-8>
- 851 Basterretxea, G., Font-Muñoz, J. S., Hernández-Carrasco, I., & Sañudo-Wilhelmy, S. A. (2023). Global
852 variability of high-nutrient low-chlorophyll regions using neural networks and wavelet coherence
853 analysis. *Ocean Science*, 19(4), 973–990. <https://doi.org/10.5194/os-19-973-2023>
- 854 Bazzani, E., Lauritano, C., & Saggiomo, M. (2023). Southern Ocean Iron Limitation of Primary Production
855 between Past Knowledge and Future Projections. *Journal of Marine Science and Engineering*, 11(2),
856 272.
- 857 Bertrand, E. M., Saito, M. A., Lee, P. A., Dunbar, R. B., Sedwick, P. N., & Ditullio, G. R. (2011). Iron
858 limitation of a springtime bacterial and phytoplankton community in the Ross Sea: Implications for
859 vitamin B12 nutrition. *Frontiers in Microbiology*, 2(AUG). Scopus.
860 <https://doi.org/10.3389/fmicb.2011.00160>
- 861 Bertrand, E. M., Saito, M. A., Rose, J. M., Riesselman, C. R., Lohan, M. C., Noble, A. E., Lee, P. A., &
862 DiTullio, G. R. (2007). Vitamin B12 and iron colimitation of phytoplankton growth in the Ross Sea.
863 *Limnology and Oceanography*, 52(3), 1079–1093.
- 864 Biggs, T. E., Alvarez-Fernandez, S., Evans, C., Mojica, K. D., Rozema, P. D., Venables, H. J., Pond, D. W., &
865 Brussaard, C. P. (2019). Antarctic phytoplankton community composition and size structure:
866 Importance of ice type and temperature as regulatory factors. *Polar Biology*, 42, 1997–2015.
- 867 Boyd, P. W. (2002). The role of iron in the biogeochemistry of the Southern Ocean and equatorial Pacific: A
868 comparison of in situ iron enrichments. *Deep Sea Research Part II: Topical Studies in Oceanography*,
869 49(9–10), 1803–1821.



- 870 Boyd, P. W., Arrigo, K. R., Strzepek, R., & Van Dijken, G. L. (2012). Mapping phytoplankton iron utilization:
871 Insights into Southern Ocean supply mechanisms. *Journal of Geophysical Research: Oceans*, *117*(C6).
- 872 Boyd, P. W., Rynearson, T. A., Armstrong, E. A., Fu, F., Hayashi, K., Hu, Z., Hutchins, D. A., Kudela, R. M.,
873 Litchman, E., & Mulholland, M. R. (2013). Marine phytoplankton temperature versus growth
874 responses from polar to tropical waters—outcome of a scientific community-wide study. *PLoS One*, *8*(5),
875 e63091.
- 876 Boyd, P. W., Strzepek, R. F., Ellwood, M. J., Hutchins, D. A., Nodder, S. D., Twining, B. S., & Wilhelm, S. W.
877 (2015). Why are biotic iron pools uniform across high- and low-iron pelagic ecosystems? *Global
878 Biogeochemical Cycles*, *29*(7), 1028–1043. <https://doi.org/10.1002/2014GB005014>
- 879 Brooks, P. R., & Crowe, T. P. (2019). Combined effects of multiple stressors: New insights into the influence of
880 timing and sequence. *Frontiers in Ecology and Evolution*, *7*, 387.
- 881 Bronselaer, B., Russell, J. L., Winton, M., Williams, N. L., Key, R. M., Dunne, J. P., Feely, R. A., Johnson, K.
882 S., & Sarmiento, J. L. (2020). Importance of wind and meltwater for observed chemical and physical
883 changes in the Southern Ocean. *Nature Geoscience*, *13*(1), 35–42. [https://doi.org/10.1038/s41561-019-
884 0502-8](https://doi.org/10.1038/s41561-019-019-0502-8)
- 885 Browning, T. J., Achterberg, E. P., Engel, A., & Mawji, E. (2021). Manganese co-limitation of phytoplankton
886 growth and major nutrient drawdown in the Southern Ocean. *Nature Communications*, *12*(1), Article 1.
887 <https://doi.org/10.1038/s41467-021-21122-6>
- 888 Buesseler, K. O., Boyd, P. W., Black, E. E., & Siegel, D. A. (2020). Metrics that matter for assessing the ocean
889 biological carbon pump. *Proceedings of the National Academy of Sciences*, *117*(18), 9679–9687.
890 <https://doi.org/10.1073/pnas.1918114117>
- 891 Burns, S. M., Bundy, R. M., Abbott, W., Abdala, Z., Sterling, A. R., Chappell, P. D., Jenkins, B. D., & Buck, K.
892 N. (2023). Interactions of bioactive trace metals in shipboard Southern Ocean incubation experiments.
893 *Limnology and Oceanography*, *68*(3), 525–543. <https://doi.org/10.1002/lno.12290>
- 894 Caron, D. A., & Hutchins, D. A. (2013). The effects of changing climate on microzooplankton grazing and
895 community structure: Drivers, predictions and knowledge gaps. *Journal of Plankton Research*, *35*(2),
896 235–252. <https://doi.org/10.1093/plankt/fbs091>
- 897 Chen, B., Landry, M. R., Huang, B., & Liu, H. (2012). Does warming enhance the effect of microzooplankton
898 grazing on marine phytoplankton in the ocean? *Limnology and Oceanography*, *57*(2), 519–526.



- 899 Cullen, J. T., & Sherrell, R. M. (1999). Techniques for determination of trace metals in small samples of size-
900 fractionated particulate matter: Phytoplankton metals off central California. *Marine Chemistry*, 67(3–
901 4), 233–247.
- 902 Cunningham, B. R., & John, S. G. (2017). The effect of iron limitation on cyanobacteria major nutrient and
903 trace element stoichiometry. *Limnology and Oceanography*, 62(2), 846–858.
904 <https://doi.org/10.1002/lno.10484>
- 905 Cutter, G. A., Andersson, P., Codispoti, L., Croot, P., Place, P., Hoe, T., Kingdom, U., Francois, R., Sciences,
906 O., Lohan, M., Circus, D., & Obata, H. (2017). *Sampling and Sample-handling Protocols for*
907 *GEOTRACES Cruises. 3.0*(August).
- 908 Darelus, E., Daae, K., Dundas, V., Fer, I., Hellmer, H. H., Janout, M., Nicholls, K. W., Sallée, J.-B., &
909 Østerhus, S. (2023). Observational evidence for on-shelf heat transport driven by dense water export in
910 the Weddell Sea. *Nature Communications*, 14(1), 1022.
- 911 De Baar, H. J. W., Boyd, P. W., Coale, K. H., Landry, M. R., Tsuda, A., Assmy, P., Bakker, D. C. E., Bozec, Y.,
912 Barber, R. T., Brzezinski, M. A., Buesseler, K. O., Boyé, M., Croot, P. L., Gervais, F., Gorbunov, M.
913 Y., Harrison, P. J., Hiscock, W. T., Laan, P., Lancelot, C., ... Wong, C. (2005). Synthesis of iron
914 fertilization experiments: From the Iron Age in the Age of Enlightenment. *Journal of Geophysical*
915 *Research: Oceans*, 110(C9), 2004JC002601. <https://doi.org/10.1029/2004JC002601>
- 916 De Baar, H. J. W., Timmermans, K. R., Laan, P., De Porto, H. H., Ober, S., Blom, J. J., Bakker, M. C.,
917 Schilling, J., Sarthou, G., Smit, M. G., & Klunder, M. (2008). Titan: A new facility for ultraclean
918 sampling of trace elements and isotopes in the deep oceans in the international Geotraces program.
919 *Marine Chemistry*, 111(1–2), 4–21. <https://doi.org/10.1016/j.marchem.2007.07.009>
- 920 De Lavergne, C., Palter, J. B., Galbraith, E. D., Bernardello, R., & Marinov, I. (2014). Cessation of deep
921 convection in the open Southern Ocean under anthropogenic climate change. *Nature Climate Change*,
922 4(4), 278–282.
- 923 Deppeler, S. L., & Davidson, A. T. (2017). Southern Ocean Phytoplankton in a Changing Climate. *Frontiers in*
924 *Marine Science*, 4. <https://www.frontiersin.org/articles/10.3389/fmars.2017.00040>
- 925 Drijfhout, S. S., Bull, C. Y. S., Hewitt, H., Holland, P. R., Jenkins, A., Mathiot, P., & Garabato, A. N. (2024).
926 An Amundsen Sea source of decadal temperature changes on the Antarctic continental shelf. *Ocean*
927 *Dynamics*, 74(1), 37–52. <https://doi.org/10.1007/s10236-023-01587-3>



- 928 Eich, C., Biggs, T. E., van de Poll, W. H., van Manen, M., Tian, H.-A., Jung, J., Lee, Y., Middag, R., &
929 Brussaard, C. P. (2022). Ecological importance of viral lysis as a loss factor of phytoplankton in the
930 Amundsen Sea. *Microorganisms*, 10(10), 1967.
- 931 Eich, C., Pont, S. B., & Brussaard, C. P. (2021). Effects of UV radiation on the chlorophyte *Micromonas polaris*
932 host–virus interactions and MpoV-45T virus infectivity. *Microorganisms*, 9(12), 2429.
- 933 Fahrbach, E., Hoppema, M., Rohardt, G., Schröder, M., & Wisotzki, A. (2004). Decadal-scale variations of
934 water mass properties in the deep Weddell Sea. *Ocean Dynamics*, 54(1), 77–91.
935 <https://doi.org/10.1007/s10236-003-0082-3>
- 936 Feng, Y., Hare, C. E., Rose, J. M., Handy, S. M., DiTullio, G. R., Lee, P. A., Smith, W. O., Peloquin, J., Tozzi,
937 S., Sun, J., Zhang, Y., Dunbar, R. B., Long, M. C., Sohst, B., Lohan, M., & Hutchins, D. A. (2010).
938 Interactive effects of iron, irradiance and CO₂ on Ross Sea phytoplankton. *Deep-Sea Research Part I:
939 Oceanographic Research Papers*, 57(3), 368–383. <https://doi.org/10.1016/j.dsr.2009.10.013>
- 940 Fisher, B. J., Poulton, A. J., Meredith, M. P., Baldry, K., Schofield, O., & Henley, S. F. (2023).
941 Biogeochemistry of climate driven shifts in Southern Ocean primary producers. *Biogeosciences
942 Discussions*, 1–29.
- 943 Fourquez, M., Janssen, D. J., Conway, T. M., Cabanes, D., Ellwood, M. J., Sieber, M., Trimborn, S., & Hassler,
944 C. (2023). Chasing iron bioavailability in the Southern Ocean: Insights from *Phaeocystis antarctica*
945 and iron speciation. *Science Advances*, 9(26), eadf9696. <https://doi.org/10.1126/sciadv.adf9696>
- 946 Friedlingstein, P., O’sullivan, M., Jones, M. W., Andrew, R. M., Gregor, L., Hauck, J., Le Quéré, C., Luijkx, I.
947 T., Olsen, A., & Peters, G. P. (2022). Global carbon budget 2022. *Earth System Science Data
948 Discussions*, 2022, 1–159.
- 949 From, N., Richardson, K., Mousing, E. A., & Jensen, P. E. (2014). Removing the light history signal from
950 normalized variable fluorescence (F_v/F_m) measurements on marine phytoplankton. *Limnology and
951 Oceanography: Methods*, 12(11), 776–783. <https://doi.org/10.4319/lom.2014.12.776>
- 952 Garrison, D. L., Gowing, M. M., Hughes, M. P., Campbell, L., Caron, D. A., Dennett, M. R., Shalapyonok, A.,
953 Olson, R. J., Landry, M. R., Brown, S. L., Liu, H.-B., Azam, F., Steward, G. F., Ducklow, H. W., &
954 Smith, D. C. (2000). Microbial food web structure in the Arabian Sea: A US JGOFS study. *Deep Sea
955 Research Part II: Topical Studies in Oceanography*, 47(7), 1387–1422. [https://doi.org/10.1016/S0967-
0645\(99\)00148-4](https://doi.org/10.1016/S0967-
956 0645(99)00148-4)



- 957 Geider, R. J. (1987). Light and temperature dependence of the carbon to chlorophyll a ratio in microalgae and
958 cyanobacteria: Implications for physiology and growth of phytoplankton. *New Phytologist*, 1–34.
- 959 Geider, R. J., & La Roche, J. (1994). The role of iron in phytoplankton photosynthesis, and the potential for
960 iron-limitation of primary productivity in the sea. *Photosynthesis Research*, 39, 275–301.
- 961 Geider, R. J., MacIntyre, H. L., & Kana, T. M. (1998). A dynamic regulatory model of phytoplanktonic
962 acclimation to light, nutrients, and temperature. *Limnology and Oceanography*, 43(4), 679–694.
- 963 Gerringa, L. J. A., Alderkamp, A.-C., Laan, P., Thuróczy, C.-E., De Baar, H. J. W., Mills, M. M., van Dijken,
964 G. L., van Haren, H., & Arrigo, K. R. (2020). Corrigendum to "Iron from melting glaciers fuels the
965 phytoplankton blooms in Amundsen Sea (Southern Ocean): Iron biogeochemistry"(Gerringa et al.,
966 2012). *Deep Sea Research Part II: Topical Studies in Oceanography*, 177, 104843.
- 967 Gerringa, L. J. A., Laan, P., Arrigo, K. R., van Dijken, G. L., & Alderkamp, A.-C. (2019). The organic
968 complexation of iron in the Ross sea. *Marine Chemistry*, 215, 103672.
969 <https://doi.org/10.1016/j.marchem.2019.103672>
- 970 Gerringa, L. J., Alderkamp, A.-C., Laan, P., Thuroczy, C.-E., De Baar, H. J., Mills, M. M., van Dijken, G. L.,
971 van Haren, H., & Arrigo, K. R. (2012). Iron from melting glaciers fuels the phytoplankton blooms in
972 Amundsen Sea (Southern Ocean): Iron biogeochemistry. *Deep Sea Research Part II: Topical Studies in*
973 *Oceanography*, 71, 16–31.
- 974 Gómez-Valdivia, F., Holland, P. R., Siahhaan, A., Dutrieux, P., & Young, E. (2023). Projected West Antarctic
975 Ocean Warming Caused by an Expansion of the Ross Gyre. *Geophysical Research Letters*, 50(6),
976 e2023GL102978. <https://doi.org/10.1029/2023GL102978>
- 977 Gordon, L. I., Jennings Jr, J. C., Ross, A. A., & Krest, J. M. (1993). A suggested protocol for continuous flow
978 automated analysis of seawater nutrients (phosphate, nitrate, nitrite and silicic acid) in the WOCE
979 Hydrographic Program and the Joint Global Ocean Fluxes Study. *WOCE Hydrographic Program*
980 *Office, Methods Manual WHPO*, 68/91, 1–52.
- 981 Greene, R. M., Geider, R. J., Kolber, Z., & Falkowski, P. G. (1992). Iron-induced changes in light harvesting
982 and photochemical energy conversion processes in eukaryotic marine algae. *Plant Physiology*, 100(2),
983 565–575.
- 984 Hassler, C. S., & Schoemann, V. (2009). Bioavailability of organically bound Fe to model phytoplankton of the
985 Southern Ocean. *Biogeosciences*, 6(10), 2281–2296.



- 986 Hawco, N. J., Tagliabue, A., & Twining, B. S. (2022). Manganese Limitation of Phytoplankton Physiology and
987 Productivity in the Southern Ocean. *Global Biogeochemical Cycles*, 36(11), e2022GB007382.
988 <https://doi.org/10.1029/2022GB007382>
- 989 Hillenbrand, C.-D., & Cortese, G. (2006). Polar stratification: A critical view from the Southern Ocean.
990 *Palaeogeography, Palaeoclimatology, Palaeoecology*, 242(3–4), 240–252.
- 991 Hinz, D. J., Nielsdóttir, M. C., Korb, R. E., Whitehouse, M. J., Poulton, A. J., Moore, C. M., Achterberg, E. P.,
992 & Bibby, T. S. (2012). Responses of microplankton community structure to iron addition in the Scotia
993 Sea. *Deep-Sea Research Part II: Topical Studies in Oceanography*, 59–60, 36–46.
994 <https://doi.org/10.1016/j.dsr2.2011.08.006>
- 995 Hopwood, M. J., Carroll, D., Höfer, J., Achterberg, E. P., Meire, L., Le Moigne, F. A., Bach, L. T., Eich, C.,
996 Sutherland, D. A., & González, H. E. (2019). Highly variable iron content modulates iceberg-ocean
997 fertilisation and potential carbon export. *Nature Communications*, 10(1), 5261.
- 998 Huang, Y., Fassbender, A. J., & Bushinsky, S. M. (2023). Biogenic carbon pool production maintains the
999 Southern Ocean carbon sink. *Proceedings of the National Academy of Sciences*, 120(18),
1000 e2217909120. <https://doi.org/10.1073/pnas.2217909120>
- 1001 Hutchins, D. A., & Boyd, P. W. (2016). Marine phytoplankton and the changing ocean iron cycle. *Nature*
1002 *Climate Change*, 6(12), 1072–1079.
- 1003 Hutchins, D. A., & Bruland, K. W. (1998). Iron-limited diatom growth and Si:N uptake ratios in a coastal
1004 upwelling regime. *Nature*, 393(6685), 561–564. Scopus. <https://doi.org/10.1038/31203>
- 1005 Jabre, L., & Bertrand, E. M. (2020). Interactive effects of iron and temperature on the growth of *Fragilariopsis*
1006 *cylindrus*. *Limnology and Oceanography Letters*, 5(5), 363–370.
- 1007 Jabre, L. J., Allen, A. E., McCain, J. S. P., McCrow, J. P., Tenenbaum, N., Spackeen, J. L., Sipler, R. E., Green,
1008 B. R., Bronk, D. A., Hutchins, D. A., & Bertrand, E. M. (2021). Molecular underpinnings and
1009 biogeochemical consequences of enhanced diatom growth in a warming Southern Ocean. *Proceedings*
1010 *of the National Academy of Sciences*, 118(30), e2107238118. <https://doi.org/10.1073/pnas.2107238118>
- 1011 Jensen, L. T., Wyatt, N. J., Landing, W. M., & Fitzsimmons, J. N. (2020). Assessment of the stability, sorption,
1012 and exchangeability of marine dissolved and colloidal metals. *Marine Chemistry*, 220, 103754.
1013 <https://doi.org/10.1016/j.marchem.2020.103754>



- 1014 Jeon, M. H., Jung, J., Park, M. O., Aoki, S., Kim, T.-W., & Kim, S.-K. (2021). Tracing Circumpolar Deep
1015 Water and glacial meltwater using humic-like fluorescent dissolved organic matter in the Amundsen
1016 Sea, Antarctica. *Marine Chemistry*, 235, 104008. <https://doi.org/10.1016/j.marchem.2021.104008>
- 1017 Kroh, G. E., & Pilon, M. (2020). Regulation of iron homeostasis and use in chloroplasts. *International Journal*
1018 *of Molecular Sciences*, 21(9), 3395.
- 1019 Krumhardt, K. M., Long, M. C., Sylvester, Z. T., & Petrik, C. M. (2022). Climate drivers of Southern Ocean
1020 phytoplankton community composition and potential impacts on higher trophic levels. *Frontiers in*
1021 *Marine Science*, 9, 916140.
- 1022 Kustka, A. B., Allen, A. E., & Morel, F. M. (2007). Sequence analysis and transcriptional regulation of iron
1023 acquisition genes in two marine diatoms 1. *Journal of Phycology*, 43(4), 715–729.
- 1024 Lampe, R. H., Mann, E. L., Cohen, N. R., Till, C. P., Thamtrakoln, K., Brzezinski, M. A., Bruland, K. W.,
1025 Twining, B. S., & Marchetti, A. (2018). Different iron storage strategies among bloom-forming
1026 diatoms. *Proceedings of the National Academy of Sciences*, 115(52), E12275–E12284.
1027 <https://doi.org/10.1073/pnas.1805243115>
- 1028 Lane, E. S., Jang, K., Cullen, J. T., & Maldonado, M. T. (2008). The interaction between inorganic iron and
1029 cadmium uptake in the marine diatom *Thalassiosira oceanica*. *Limnology and Oceanography*, 53(5),
1030 1784–1789.
- 1031 Lannuzel, D., Vancoppenolle, M., van Der Merwe, P., De Jong, J., Meiners, K. M., Grotti, M., Nishioka, J., &
1032 Schoemann, V. (2016). Iron in sea ice: Review and new insights. *Elementa*, 4, 000130.
- 1033 Laws, E. A., & Bannister, T. T. (1980). Nutrient-and light-limited growth of *Thalassiosira fluviatilis* in
1034 continuous culture, with implications for phytoplankton growth in the ocean 1. *Limnology and*
1035 *Oceanography*, 25(3), 457–473.
- 1036 Maat, D. S., Biggs, T., Evans, C., Van Bleijswijk, J. D. L., Van der Wel, N. N., Dutilh, B. E., & Brussaard, C. P.
1037 D. (2017). Characterization and Temperature Dependence of Arctic *Micromonas polaris* Viruses.
1038 *Viruses*, 9(6), Article 6. <https://doi.org/10.3390/v9060134>
- 1039 Mackey, M. D., Mackey, D. J., Higgins, H. W., & Wright, S. W. (1996). CHEMTAX—a program for estimating
1040 class abundances from chemical markers: Application to HPLC measurements of phytoplankton.
1041 *Marine Ecology Progress Series*, 144, 265–283.
- 1042 Marie, D., Partensky, F., Vaulot, D., & Brussaard, C. P. D. (1999). Enumeration of phytoplankton, bacteria, and
1043 viruses in marine samples. *Current Protocols in Cytometry*. <https://doi.org/10.1002/0471142956>



- 1044 Martin, J. H., Fitzwater, S. E., & Gordon, R. M. (1990). Iron deficiency limits phytoplankton growth in
1045 Antarctic waters. *Global Biogeochemical Cycles*, 4(1), 5–12.
- 1046 McCain, J. S. P., Tagliabue, A., Susko, E., Achterberg, E. P., Allen, A. E., & Bertrand, E. M. (2021). Cellular
1047 costs underpin micronutrient limitation in phytoplankton. *Science Advances*, 7(32), eabg6501.
1048 <https://doi.org/10.1126/sciadv.abg6501>
- 1049 Meredith, M., M. Sommerkorn, S. Cassotta, C. Derksen, A. Ekaykin, A. Hollowed, G. Kofinas, A. Mackintosh,
1050 J. Melbourne-Thomas, M.M.C. Muelbert, G. Ottersen, H. Pritchard, and E.A.G. Schuur. (2019).
1051 *Chapter 3: IPCC Polar regions — Special Report on the Ocean and Cryosphere in a Changing*
1052 *Climate*. <https://www.ipcc.ch/srocc/chapter/chapter-3-2/>
- 1053 Meyerink, S. W., Ellwood, M. J., Maher, W. A., Dean Price, G., & Strzepek, R. F. (2017). Effects of iron
1054 limitation on silicon uptake kinetics and elemental stoichiometry in two Southern Ocean diatoms,
1055 *Eucampia antarctica* and *Proboscia inermis*, and the temperate diatom *Thalassiosira pseudonana*.
1056 *Limnology and Oceanography*, 62(6), 2445–2462.
- 1057 Middag, R., De Baar, H. J., Bruland, K. W., & Van Heuven, S. M. (2020). The distribution of nickel in the
1058 West-Atlantic Ocean, its relationship with phosphate and a comparison to cadmium and zinc. *Frontiers*
1059 *in Marine Science*, 7, 105.
- 1060 Middag, R., Zitoun, R., & Conway, T. (2023). Trace Metals. In J. Blasco & A. Tovar-Sánchez (Eds.), *Marine*
1061 *Analytical Chemistry* (pp. 103–198). Springer International Publishing. [https://doi.org/10.1007/978-3-](https://doi.org/10.1007/978-3-031-14486-8_3)
1062 [031-14486-8_3](https://doi.org/10.1007/978-3-031-14486-8_3)
- 1063 Mills, M. M., Alderkamp, A. C., Thuróczy, C. E., van Dijken, G. L., Laan, P., de Baar, H. J. W., & Arrigo, K.
1064 R. (2012). Phytoplankton biomass and pigment responses to Fe amendments in the Pine Island and
1065 Amundsen polynyas. *Deep-Sea Research Part II: Topical Studies in Oceanography*, 71–76(3), 61–76.
1066 <https://doi.org/10.1016/j.dsr2.2012.03.008>
- 1067 Minas, H. J., & Minas, M. (1992). Net community production in High nutrient-low chlorophyll waters of the
1068 tropical and Antarctic oceans-grazing vs iron hypothesis. *Oceanologica Acta*, 15(2), 145–162.
- 1069 Moore, J. K., Fu, W., Primeau, F., Britten, G. L., Lindsay, K., Long, M., Doney, S. C., Mahowald, N., Hoffman,
1070 F., & Randerson, J. T. (2018). Sustained climate warming drives declining marine biological
1071 productivity. *Science*, 359(6380), 1139–1143. <https://doi.org/10.1126/science.aao6379>



- 1072 Morán, X. A. G., Sebastián, M., Pedrís-Alió, C., & Estrada, M. (2006). Response of Southern Ocean
1073 phytoplankton and bacterioplankton production to short-term experimental warming. *Limnology and*
1074 *Oceanography*, 51(4), 1791–1800. <https://doi.org/10.4319/lo.2006.51.4.1791>
- 1075 Morrison, A. K., England, M. H., Hogg, A. McC., & Kiss, A. E. (2023). Weddell Sea Control of Ocean
1076 Temperature Variability on the Western Antarctic Peninsula. *Geophysical Research Letters*, 50(15),
1077 e2023GL103018. <https://doi.org/10.1029/2023GL103018>
- 1078 Noiri, Y., Kudo, I., Kiyosawa, H., Nishioka, J., & Tsuda, A. (2005). Influence of iron and temperature on
1079 growth, nutrient utilization ratios and phytoplankton species composition in the western subarctic
1080 Pacific Ocean during the SEEDS experiment. *Progress in Oceanography*, 64(2–4), 149–166.
1081 <https://doi.org/10.1016/j.pocean.2005.02.006>
- 1082 Ohnemus, D. C., Auro, M. E., Sherrell, R. M., Lagerström, M., Morton, P. L., Twining, B. S., Rauschenberg, S.,
1083 & Lam, P. J. (2014). Laboratory intercomparison of marine particulate digestions including Piranha: A
1084 novel chemical method for dissolution of polyethersulfone filters. *Limnology and Oceanography:*
1085 *Methods*, 12(8), 530–547.
- 1086 Olson, R. J., Sosik, H. M., Chekalyuk, A. M., & Shalapyonok, A. (2000). Effects of iron enrichment on
1087 phytoplankton in the Southern Ocean during late summer: Active fluorescence and flow cytometric
1088 analyses. *Deep-Sea Research Part II: Topical Studies in Oceanography*, 47(15–16), 3181–3200.
1089 Scopus. [https://doi.org/10.1016/S0967-0645\(00\)00064-3](https://doi.org/10.1016/S0967-0645(00)00064-3)
- 1090 Pausch, F., Bischof, K., & Trimborn, S. (2019). Iron and manganese co-limit growth of the Southern Ocean
1091 diatom *Chaetoceros debilis*. *PLOS ONE*, 14(9), e0221959.
1092 <https://doi.org/10.1371/journal.pone.0221959>
- 1093 Peers, G., & Price, N. M. (2004). A role for manganese in superoxide dismutases and growth of iron-deficient
1094 diatoms. *Limnology and Oceanography*, 49(5), 1774–1783. <https://doi.org/10.4319/lo.2004.49.5.1774>
- 1095 Planquette, H., & Sherrell, R. M. (2012). Sampling for particulate trace element determination using water
1096 sampling bottles: Methodology and comparison to in situ pumps. *Limnology and Oceanography:*
1097 *Methods*, 10(5), 367–388.
- 1098 Primeau, F. W., Holzer, M., & DeVries, T. (2013). Southern Ocean nutrient trapping and the efficiency of the
1099 biological pump. *Journal of Geophysical Research: Oceans*, 118(5), 2547–2564.
1100 <https://doi.org/10.1002/jgrc.20181>



- 1101 R Core Team. (2021). *R: A language and environment for statistical computing*. (4.1.0). R Foundation for
1102 Statistical Computing.
- 1103 Reay, D. S., Priddle, J., Nedwell, D. B., Whitehouse, M. J., Ellis-Evans, J. C., Deubert, C., & Connelly, D. P.
1104 (2001). Regulation by low temperature of phytoplankton growth and nutrient uptake in the Southern
1105 Ocean. *Marine Ecology Progress Series*, 219, 51–64.
- 1106 Rignot, E., Jacobs, S., Mouginot, J., & Scheuchl, B. (2013). Ice-Shelf Melting Around Antarctica. *Science*,
1107 341(6143), 266–270. <https://doi.org/10.1126/science.1235798>
- 1108 Rijkenberg, M. J. A., de Baar, H. J. W., Bakker, K., Gerringa, L. J. A., Keijzer, E., Laan, M., Laan, P., Middag,
1109 R., Ober, S., van Ooijen, J., Ossebaar, S., van Weerlee, E. M., & Smit, M. G. (2015). ‘PRISTINE’, a
1110 new high volume sampler for ultraclean sampling of trace metals and isotopes. *Marine Chemistry*,
1111 177(October 2017), 501–509. <https://doi.org/10.1016/j.marchem.2015.07.001>
- 1112 Rose, J. M., Feng, Y., DiTullio, G. R., Dunbar, R. B., Hare, C. E., Lee, P. A., Lohan, M., Long, M., Smith Jr,
1113 W. O., & Sohst, B. (2009). Synergistic effects of iron and temperature on Antarctic phytoplankton and
1114 microzooplankton assemblages. *Biogeosciences*, 6(12), 3131–3147.
- 1115 Ryan-Keogh, T. J., Thomalla, S. J., Monteiro, P. M., & Tagliabue, A. (2023). Multidecadal trend of increasing
1116 iron stress in Southern Ocean phytoplankton. *Science*, 379(6634), 834–840.
- 1117 Ryderheim, F., Grønning, J., & Kiørboe, T. (2022). Thicker shells reduce copepod grazing on diatoms.
1118 *Limnology and Oceanography Letters*, 7(5), 435–442.
- 1119 Sarmiento, J. L., Gruber, N., Brzezinski, M. A., & Dunne, J. P. (2004). High-latitude controls of thermocline
1120 nutrients and low latitude biological productivity. *Nature*, 427(6969), Article 6969.
1121 <https://doi.org/10.1038/nature02127>
- 1122 Scharek, R., Van Leeuwe, M. A., & De Baar, H. J. W. (1997). Responses of Southern Ocean phytoplankton to
1123 the addition of trace metals. *Deep-Sea Research Part II: Topical Studies in Oceanography*, 44(1–2),
1124 209–227. [https://doi.org/10.1016/S0967-0645\(96\)00074-4](https://doi.org/10.1016/S0967-0645(96)00074-4)
- 1125 Schoffman, H., Lis, H., Shaked, Y., & Keren, N. (2016). Iron–Nutrient Interactions within Phytoplankton.
1126 *Frontiers in Plant Science*, 7. <https://www.frontiersin.org/articles/10.3389/fpls.2016.01223>
- 1127 Selz, V., Lowry, K. E., Lewis, K. M., Joy-Warren, H. L., van de Poll, W., Nirmel, S., Tong, A., & Arrigo, K. R.
1128 (2018). Distribution of Phaeocystis antarctica-dominated sea ice algal communities and their potential
1129 to seed phytoplankton across the western Antarctic Peninsula in spring. *Marine Ecology Progress
1130 Series*, 586, 91–112.



- 1131 Seyitmuhammedov, K., Stirling, C. H., Reid, M. R., van Hale, R., Laan, P., Arrigo, K. R., van Dijken, G.,
1132 Alderkamp, A.-C., & Middag, R. (2022). The distribution of Fe across the shelf of the Western
1133 Antarctic Peninsula at the start of the phytoplankton growing season. *Marine Chemistry*, 238, 104066.
1134 Sherrell, R. M., Lagerström, M. E., Forsch, K. O., Stammerjohn, S. E., & Yager, P. L. (2015). Dynamics of
1135 dissolved iron and other bioactive trace metals (Mn, Ni, Cu, Zn) in the Amundsen Sea Polynya,
1136 Antarctica. *Elementa: Science of the Anthropocene*, 3, 000071.
1137 <https://doi.org/10.12952/journal.elementa.000071>
1138 Shi, J.-R., Talley, L. D., Xie, S.-P., Liu, W., & Gille, S. T. (2020). Effects of buoyancy and wind forcing on
1139 Southern Ocean climate change. *Journal of Climate*, 33(23), 10003–10020.
1140 Slagter, H. A., Gerringa, L. J. A., & Brussaard, C. P. D. (2016). Phytoplankton Virus Production Negatively
1141 Affected by Iron Limitation. *Frontiers in Marine Science*, 3.
1142 <https://www.frontiersin.org/articles/10.3389/fmars.2016.00156>
1143 Stapleford, L. S., & Smith, R. E. (1996). The interactive effects of temperature and silicon limitation on the
1144 psychrophilic ice diatom *Pseudonitzschia seriata*. *Polar Biology*, 16, 589–594.
1145 Tagliabue, A., Aumont, O., DeAth, R., Dunne, J. P., Dutkiewicz, S., Galbraith, E., Misumi, K., Moore, J. K.,
1146 Ridgwell, A., Sherman, E., Stock, C., Vichi, M., Völker, C., & Yool, A. (2016). How well do global
1147 ocean biogeochemistry models simulate dissolved iron distributions? *Global Biogeochemical Cycles*,
1148 30(2), 149–174. <https://doi.org/10.1002/2015GB005289>
1149 Tagliabue, A., Sallée, J.-B., Bowie, A. R., Lévy, M., Swart, S., & Boyd, P. W. (2014). Surface-water iron
1150 supplies in the Southern Ocean sustained by deep winter mixing. *Nature Geoscience*, 7(4), 314–320.
1151 Takahashi, T., Sweeney, C., Hales, B., Chipman, D. W., Newberger, T., Goddard, J. G., Iannuzzi, R. A., &
1152 Sutherland, S. C. (2012). The changing carbon cycle in the Southern Ocean. *Oceanography*, 25(3), 26–
1153 37.
1154 Teske, V., Timmermann, R., & Semmler, T. (2024). Subsurface warming in the Antarctica’s Weddell Sea can
1155 be avoided by reaching the 2°C warming target. *Communications Earth & Environment*, 5(1), 93.
1156 Thomalla, S. J., Nicholson, S.-A., Ryan-Keogh, T. J., & Smith, M. E. (2023). Widespread changes in Southern
1157 Ocean phytoplankton blooms linked to climate drivers. *Nature Climate Change*, 13(9), 975–984.
1158 Twining, B. S., Baines, S. B., & Fisher, N. S. (2004). Element stoichiometries of individual plankton cells
1159 collected during the Southern Ocean Iron Experiment (SOFEX). *Limnology and Oceanography*, 49(6),
1160 2115–2128. <https://doi.org/10.4319/lo.2004.49.6.2115>



- 1161 Van der Merwe, P., Wuttig, K., Holmes, T., Trull, T. W., Chase, Z., Townsend, A. T., Goemann, K., & Bowie,
1162 A. R. (2019). High lability Fe particles sourced from glacial erosion can meet previously unaccounted
1163 biological demand: Heard Island, Southern Ocean. *Frontiers in Marine Science*, 6, 332.
- 1164 Van Heukelem, L., & Thomas, C. S. (2001). Computer-assisted high-performance liquid chromatography
1165 method development with applications to the isolation and analysis of phytoplankton pigments. *Journal*
1166 *of Chromatography A*, 910(1), 31–49. [https://doi.org/10.1016/S0378-4347\(00\)00603-4](https://doi.org/10.1016/S0378-4347(00)00603-4)
- 1167 Van Manen, M., Aoki, S., Brussaard, C. P., Conway, T. M., Eich, C., Gerringa, L. J., Jung, J., Kim, T.-W., Lee,
1168 S., & Lee, Y. (2022). The role of the Dotson Ice Shelf and Circumpolar Deep Water as driver and
1169 source of dissolved and particulate iron and manganese in the Amundsen Sea polynya, Southern
1170 Ocean. *Marine Chemistry*, 246, 104161.
- 1171 Veldhuis, M. J., & Kraay, G. W. (2004). Phytoplankton in the subtropical Atlantic Ocean: Towards a better
1172 assessment of biomass and composition. *Deep Sea Research Part I: Oceanographic Research Papers*,
1173 51(4), 507–530.
- 1174 Venables, H., & Moore, C. M. (2010). Phytoplankton and light limitation in the Southern Ocean: Learning from
1175 high-nutrient, high-chlorophyll areas. *Journal of Geophysical Research: Oceans*, 115(C2).
- 1176 Verardo, D. J., Froelich, P. N., & McIntyre, A. (1990). Determination of organic carbon and nitrogen in marine
1177 sediments using the Carlo Erba NA-1500 Analyzer. *Deep Sea Research Part A. Oceanographic*
1178 *Research Papers*, 37(1), 157–165.
- 1179 Viljoen, J. J., Philibert, R., Van Horsten, N., Mtshali, T., Roychoudhury, A. N., Thomalla, S., & Fietz, S.
1180 (2018). Phytoplankton response in growth, photophysiology and community structure to iron and light
1181 in the Polar Frontal Zone and Antarctic waters. *Deep-Sea Research Part I: Oceanographic Research*
1182 *Papers*, 141, 118–129. Scopus. <https://doi.org/10.1016/j.dsr.2018.09.006>
- 1183 Waite, A. M., & Nodder, S. D. (2001). The effect of in situ iron addition on the sinking rates and export flux of
1184 Southern Ocean diatoms. *Deep Sea Research Part II: Topical Studies in Oceanography*, 48(11–12),
1185 2635–2654.
- 1186 Wang, X. J., Behrenfeld, M., Le Borgne, R., Murtugudde, R., & Boss, E. (2009). Regulation of phytoplankton
1187 carbon to chlorophyll ratio by light, nutrients and temperature in the Equatorial Pacific Ocean: A basin-
1188 scale model. *Biogeosciences*, 6(3), 391–404.



- 1189 Worden, A. Z., Nolan, J. K., & Palenik, B. (2004). Assessing the dynamics and ecology of marine
1190 picophytoplankton: The importance of the eukaryotic component. *Limnology and Oceanography*,
1191 49(1), 168–179. <https://doi.org/10.4319/lo.2004.49.1.0168>
- 1192 Wu, M., McCain, J. S. P., Rowland, E., Middag, R., Sandgren, M., Allen, A. E., & Bertrand, E. M. (2019a).
1193 Manganese and iron deficiency in Southern Ocean *Phaeocystis antarctica* populations revealed through
1194 taxon-specific protein indicators. *Nature Communications*, 10(1), 3582.
1195 <https://doi.org/10.1038/s41467-019-11426-z>
- 1196 Yoon, J.-E., Yoo, K.-C., Macdonald, A. M., Yoon, H.-I., Park, K.-T., Yang, E. J., Kim, H.-C., Lee, J. I., Lee, M.
1197 K., Jung, J., Park, J., Lee, J., Kim, S., Kim, S.-S., Kim, K., & Kim, I.-N. (2018). Reviews and
1198 syntheses: Ocean iron fertilization experiments – past, present, and future looking to a future Korean
1199 Iron Fertilization Experiment in the Southern Ocean (KIFES) project. *Biogeosciences*, 15(19), 5847–
1200 5889. <https://doi.org/10.5194/bg-15-5847-2018>
- 1201 Zhu, Z., Xu, K., Fu, F., Spackeen, J. L., Bronk, D. A., & Hutchins, D. A. (2016). A comparative study of iron
1202 and temperature interactive effects on diatoms and *Phaeocystis antarctica* from the Ross Sea,
1203 Antarctica. *Marine Ecology Progress Series*, 550, 39–51.
- 1204